UNIVERSIDADE DE LISBOA

FACULDADE DE CIÊNCIAS

DEPARTAMENTO DE FÍSICA

CONTROLLING SUPERPARAMAGNETIC PARTICLES WITH DYNAMIC MAGNETIC FIELDS GENERATED BY A HELMHOLTZ-COIL SYSTEM

Rui Pedro Rodrigues Caldeira

Mestrado em Engenharia Física

2010

UNIVERSIDADE DE LISBOA
FACULDADE DE CIÊNCIAS
DEPARTAMENTO DE FÍSICA

CONTROLLING SUPERPARAMAGNETIC PARTICLES WITH
DYNAMIC MAGNETIC FIELDS GENERATED BY A HELMHOLTZ-COIL SYSTEM

Rui Pedro Rodrigues Caldeira

Mestrado em Engenharia Física

Dissertação Orientada pelos Professores Doutores:

Claus Fütterer (Universidade de Leipzig)

Guiomar Evans (Universidade de Lisboa)

2010

Abstract

Controlling superparamagnetic particles with dynamic magnetic fields generated by a Helmholtz-coil system

The aim of this work was the creation of a novel system of magnetic tweezers which is surface free and makes possible the massive parallel measurement of macromolecule characteristics. The system is able to magnetically control superparamagnetic microparticles which control macromolecules, DNA strands or cells attached to them in a surface free environment, i.e. without the use of surfaces to which the objects are bond. This allows the system composed by a pair of beads and macromolecule to float freely in the solution, allowing parallel and inside cell measurements.

The system constructed is composed of two pairs of water cooled Helmholtz coils controlled by an electronic circuit and software. The system is mounted on an inverted fluorescence microscope. The magnetic forces acting on different types of particles were calculated and fully simulated. This allowed the optimization of the coils' parameters.

In the present document we explain the physical concepts behind the behavior of the magnetic particles, the details of the design, fabrication and specifications of the control system and at the end we show and discuss some qualitative experiments made with the system.

Keywords: magnetic tweezers, magnetic microparticles, superparamagnetism, helmholtz coil, digital electronic control, computerized control, cell manipulation, rheology.

Sumário

Controlo de partículas superparamagnéticas com campos magnéticos dinâmicos gerados por um sistema de bobinas de Helmholtz

O objectivo deste trabalho foi a criação de um novo sistema de pinças magnéticas que funciona livre de superfícies e possibilita a medição paralela (ou massiva) de características de macromoléculas. O sistema é capaz de controlar magneticamente micropartículas superparamagnéticas que controlam macromoléculas, pequenas sequências de DNA ou células a elas acopladas num ambiente livre de superfícies, o que significa sem o uso de um sitema físico para os fixar. Isto permite ao sistema composto por um par de partículas magnéticas e macromolécula flutuar livremente na solução, permitindo medições paralelas e dentro de células.

O sistema é composto por dois pares de bobinas de Helmholtz arrefecidas a água, controladas por um sistema electrónico e um programa especificamente projectados para a função. O sistema está montado num microscópio invertido com capacidade para microscopia de fluorescência. As forças magnéticas que actuam nos diferentes tipos de micropartículas magnéticas foram calculadas e simuladas o que permitiu uma optimização dos parâmetros das bobinas.

No presente documento explicamos os conceitos físicos intervenientes no comportamento das partículas magnéticas, os detalhes do desenho, construção e especificações do sistema de controlo e no fim mostramos e discutimos algumas experiências qualitativas.

Palavras-chave: pinças magnéticas, micropartículas magnéticas, superparamagnetismo, bobina de helmholtz, controlo electrónico digital, controlo automático, manipulação de células, reologia.

Acknowledgements

For the present work I thank the ever questioning and open spirit of Professor Claus Fütterer. The perseverance, help and understanding of Professors Margarida Godinho, Guiomar Evans and José Augusto. The work and patience in understanding my broken german of the Workshop Staff and PWM department at the Physics Faculty of the University of Leipzig. All my friends in Portugal for always being there, even though so far away: Jorge (o meu procurador mais que tudo!), Marta (a minha mais Mimosa), Ana (por dizer que se lembra de mim), Inês (pelas curtas conversas ao telefone), Joel (por me querer vir visitar. Ah! Tens de pagar uma mini ao Ricardo Pratas), Quarenta (por gostar de mim incondicionalmente), Filipe (por tocar comigo via internets), Tiago (por me dar coisas para me distrair), Caeli (pelos Oquestrada), Catarina (por estar a safar-se num sítio mais frio do que o meu), Sílvia (a verdadeira Bobina) and Nuno (por ter uma barba à maneira) for the lovely visit, Elias (pelos sábios conselhos), Paulo (por me dizer 'isso é normal man'), Len (por dizer que tem saudades minhas), David (o Batista, he also visited me!), David (o Raposo, por ainda me achar piada), to my hometown friends, Nuno, Zé, Tiago, Rei, Nelson, Gonçalo, and all of you for showing me that friendship doesn't fade with time nor distance. All my friends in Germany and surrounding countries for always being here and oh so close: Diogo, Lisa, Katharina, Pedro, Michael, Rita, Marta, Nuno, Joana e Carolina, David e Inês, Francis (for the superfly AFM and MFM) and Josepha (die Sephinha). I also thank all the friends I forgot to mention (I'm writing this two days before delivery and I still have to write the conclusion!).

All my family, specially Ana, Cândida and Rui for giving me the courage, motivation and possibility of making this adventure.

Contents

List of Figures

Glossary

LabVIEW Laboratory Virtual Instrumentation Engineering Workbench

bead Superparamagnetic microparticles

PWM Pulse Width Modulation

MOSFET Metal Oxide Semiconductor Field Effect Transistor

DNA Deoxyribonucleic acid

mRNA Messenger Ribonucleic acid

PMMA Poly(methyl methacrylate)

PS Polystyrene

AFM Atomic Force Microscopy

MFM Magnetic Force Microscopy

Epoxy Polymer formed from a reaction of epoxide and polyamine

GUI Graphic User Interface

PC Personal Computer

USB Universal Serial Bus

DAQ Data acquisition device

N North

NE Northeast

E East

SE Southeast

S South

SW Southwest

W West

WNW West-Northwest

NW Northwest

1

Introduction

The aim of this work is to create a new system capable of controlling superparamagnetic microparticles and in a near future use this capability, and the possibility of connecting the beads to the biological objects, to move, rotate, vibrate, twist, break, push and pull biological objects such as DNA (Deoxyribonucleic Acid) strands and other macromolecules, different cell types and microorganisms.

The study of the cell's and macromolecule's mechanical properties has become a major theme of research in the modern and contemporary biophysics. The journals are devoting a lot of attention to this emerging field and the number of researchers dedicated to it increases every year.

The manipulation of individual entities is very attractive to the scientist. The main goal is to characterize and understand the function of all constituent parts of living organisms and with this gathered knowledge advance in the understanding of the mechanisms of life. Applying physical knowledge to a biological system is something that permits the study of the kinetics of molecular motors, the folding of biomolecules such as proteins and DNA, the viscoelastic and rheological (flow of matter) properties of the cell, the transport of matter through pores of channels, the physical properties of membranes and the structure of biological networks, among many other examples.

One can fairly say that these studies will continue to make the relation between physics and biology closer and closer.

1.1   Motivation

The idea of constructing a system from ground up was to me always a very fascinating one. Making an idea real and functioning or even understanding why it is not possible is the part that most interests me.

Professor Claus offered, in a Biophysics class, the opportunity to work with him in the development of a new system and latter in its use. At the time, looking for a Master Thesis it caught my interested. After the first meetings I knew this was a project for me and jumped right in. The multidisciplinary aspect of the work got me hooked. The possibility of developing a system that requires knowledge from different fields of Physics and also from Electronics and even Programming, gave me the justification for my Physics Engineering studies until now. The challenge was laid on the table and we took it.

From an empty table top, we managed to create a system capable of controlling microparticles and even cells and microorganisms. The different modes of controlling the particles, or of orienting the magnetic field, with such simple electronics was to us the most surprising aspect of it all. Parallel to its simplicity is its low cost which plays an evermore important role in physical research laboratories where the funding is not abundant.

1.2   State of the Art

A magnetic tweezer is a technique based on the principle that a force can be applied on a magnetized microparticle when in the presence of a magnetic field gradient:

$$F = -\mu \nabla B \tag{1.1}$$

where μ is the magnetic permeability of the material and ∇B is the gradient of the magnetic field.

A possible configuration is shown in figure 1.1.a. The microparticle is hold in the magnetic field gradient generated by the two permanent magnets. Macromolecules are then bond to a glass surface and to the surface of the particle. The molecule is then pulled by translating the magnets, increasing or decreasing the gradient and the force. The range of forces one achieves is in the order of 10^{-2} to 10 pN [1], these forces depend
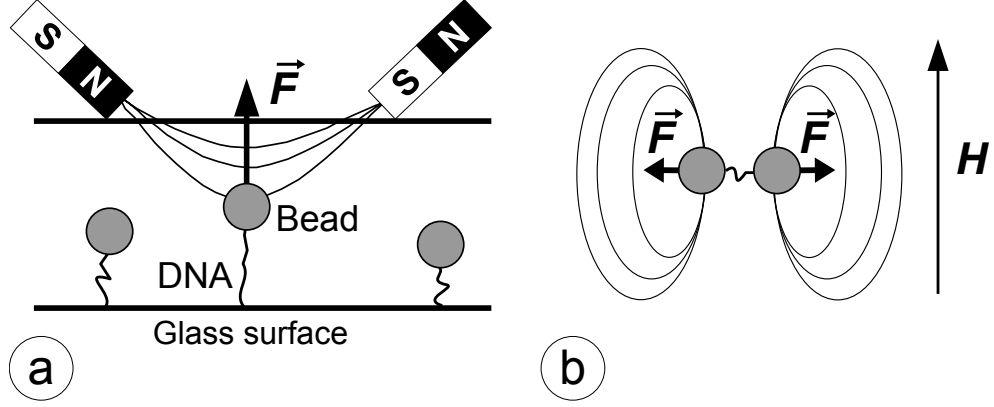
Figure 1.1: Different configurations for a magnetic tweezer system: (a) Possible 'classical' configuration for a magnetic tweezer. Note that the pulling force derives from the gradient of an inhomogeneous field formed by the two permanent magnets. (b) The configuration of our magnetic tweezer. The gradient is generated by the stray induction field of each magnetic particle.

greatly on the magnetic field's intensity and on the size of the magnetic particles.

Our system differs from this configuration in the way that no glass surface is needed (see figure 1.1.b). The macromolecule is bond at both ends to two different magnetic particles. These particles float freely in the solution. The magnetic field produced by a pair of Helmholtz coils induces a stray magnetic field on both magnetic particles and these will then spread apart due to the forces derived from the local inhomogeneous magnetic field. The forces achieved are of the same order and can be increased, with the increasing of the applied magnetic field's intensity.

1.3   Thesis Structure

In this work we begin by explaining the fundamental *Physical Concepts* behind the system's workings such as the magnetic fields generated by it, what is magnetization and magnetic moment, what is this special form of magnetism known as superparamagnetism and why is it needed on our system, the devices used, the Helmholtz coils and the physics behind the microparticles characteristic behavior in the presence of magnetic fields, such as the magnetic forces produced between two of these particles

and their movement.

In the following chapter we describe the *Design of the System*. We begin by its structure and specifications and continue with the cooling system, the uniformity of the fields produced and their intensity and temperature dependence and end with its control. After that, the developed electronics and software associated to the system control are presented.

To end the document and prior to the final conclusions we show and briefly discuss some *Experiments and Results*. These experiments were made in a qualitative way as the system of analysis is developed at the time and are made to show the capability of the system and what it has to offer in terms of microparticle and basic biological objects control.

2

Physical Concepts

The development of this system required knowledge from different fields of Physics. Specifically on this work, we used knowledge that goes from the basic assumptions of Thermodynamics (heating and cooling of the coils), to Electromagnetism (magnetic fields produced by the coils, their interaction with the superparamagnetic microparticles), on to Mechanical Design (design of the coils, microscope table support and sample moving table), a dive into Electronics (current flow controlling circuit) and a final stop at Programming (control of electronic circuit via LabVIEW[1]).

Using the system took us on a new path, with new paradigms and a peek into the unusual and Brownian motion dominated world of cells and molecules.

2.1   Electromagnetism

Electromagnetism is magic. It's an invisible force that is so hard to picture and understand and of course, to explain, as is beautiful, challenging and useful. It is one of the four fundamental interactions. When we have two electrically charged particles, electromagnetism is the interaction between them. It is responsible for a lot of phenomena, from the force between electrons and protons that holds atoms together, to the electric shock we receive from a friend that is wearing a wool sweater on a dry day. It is the relationship between electric currents and magnetic fields and in this work it is responsible for the motion control of superparamagnetic microparticles.

---

[1]LabVIEW is a platform and development environment for G, a visual programming language from National Instruments.
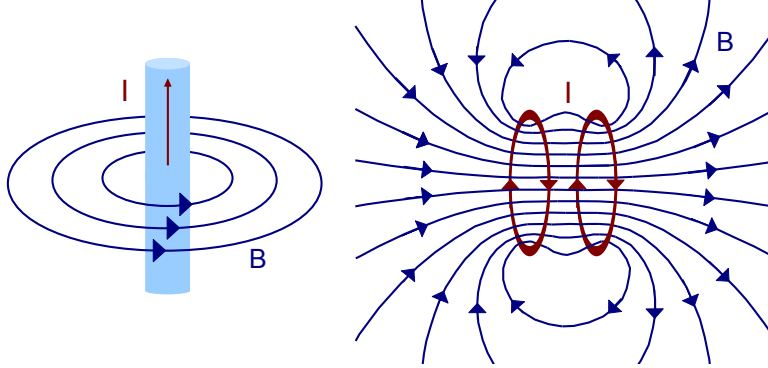
Figure 2.1: On the left we have the magnetic field produced by current on a straight wire. On the right we have a situation that more interests our work, the magnetic field produced by current on a coiled wire. In this example disposed as a Helmholtz coil.

2.2 Electric and Magnetic Fields

In the second half of the 19th century, James Clerk Maxwell published the famous Maxwell's Equations [3], as shown in 2.1 to 2.4. These are four partial differential equations that describe how the electric and magnetic fields relate to their sources, charge density and current density, and their development with time:

$$\nabla \cdot \mathbf{D} = \rho_{ext} \tag{2.1}$$

$$\nabla \cdot \mathbf{B} = 0 \tag{2.2}$$

$$\nabla \times \mathbf{E} = -\frac{\partial \mathbf{B}}{\partial t} \tag{2.3}$$

$$\nabla \times \mathbf{H} = \mathbf{J} + \frac{\partial \mathbf{D}}{\partial t} \tag{2.4}$$

where $\mathbf{E}$ is the electric field, $\mathbf{B}$ is the magnetic field (the one that interests us), $\mathbf{D}$ is the electric displacement field, $\mathbf{H}$ the magnetizing field, $\mathbf{J}$ is the total current density and ρ_{ext} is the free charge density.

While the electric field appears when a difference in electric potential is made between two points, a magnetic field appears when a current is made to flow inside a conductor. In our work the electric field eventually produced by the changing magnetic field is not taken into account and so we are only interested in the latter. For a conductor we use a copper wire, disposed in a special way, a Helmholtz coil (see figure 2.4).

A magnetic field exerts a torque on a magnetic object when the object is inside the field. This is characterized by a strength and a direction. The strength is calculated, for constant current, using the Biot-Savart law [4]:

$$\mathbf{B} = \int \frac{\mu_0}{4\pi} \frac{I d\mathbf{l} \times \hat{\mathbf{r}}}{|r|^2},$$

(2.5)

where I is the current, dl is a vector with magnitude equal to the length of the differential element of the wire and direction of the current, $\mathbf{B}$ is the strength of the magnetic field, μ_0 is the magnetic constant and $\hat{\mathbf{r}}$ is the displacement unit vector in the direction pointing from the wire element towards the point at which the field is being calculated.

The direction of the current or the field can be determined using the right hand rule as showed in figure 2.1.

When the current passes through a straight wire, its direction is represented by the thumb (red line arrow) and the field lines by the bent fingers (blue circular arrows).

When the current passes through a loop, as showed on the right side of figure 2.1, the thumb represents the direction of the magnetic field lines at the center of the coil. In the figure we can see that the magnetic field lines on the center of the apparatus (between the two coils) are parallel to each other. This means the gradient of the field is zero and so no force is exerted on a magnetic object there located. We call this homogeneity (uniformity) of the field and it interests us because of the peculiarity of behavior of the superparamagnetic particles, as we will explain later.

2.3   Magnetization and Magnetic Moment

The magnetic moment of a particle is a quantity that determines the torque that a magnetic field will exert on it. Everything that is magnetized has a magnetic moment. This moment is characterized by a magnitude (see Curie Law, equation 2.7) and a direction, the same as the magnetic field. In our case the magnetic dipole moment of the superparamagnetic particle (superparamagnetism will be explained right away in section 2.4) placed in a magnetizing field $\mathbf{H}$ will create a stray magnetic induction in its surroundings (see figure 2.2 and equation 2.6).
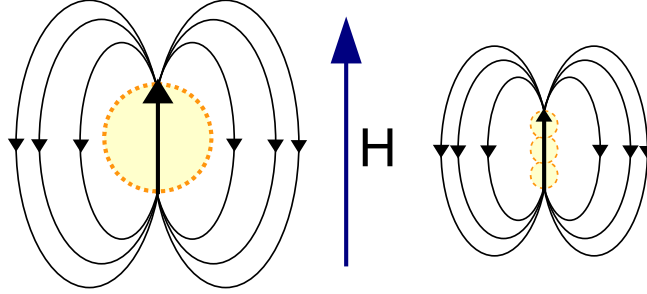
Figure 2.2: On the left, the magnetic dipole moment on a superparamagnetic particle created by a magnetizing field. The magnetic dipole moment **m** leads to a stray magnetic induction (see equation 2.6). On the right the agglomeration of various particles resulting from the stray magnetic induction.

The Stray magnetic induction is responsible, as later shown (figure 4.7 on page 47), for the formation of columns and sheets by the microparticles [5]:

$$\mathbf{B}(\mathbf{r}) = \frac{1}{4\pi}[-\frac{\mathbf{m}}{r^3} + \frac{3(\mathbf{m}.\mathbf{r})\mathbf{r}}{r^5}] \tag{2.6}$$

where **B** is the magnetic field, **m** is the dipole moment and **r** is the radius vector with r its amplitude.

2.4 Superparamagnetism

Superparamagnetism is a special form of magnetism. It appears in very small ferromagnetic particles, assumed to be spherical with a diameter up to 6 nm at room temperature [5]. In particles of this size range, the magnetization randomly flips direction influenced by temperature. The time it takes for this flip to occur is called *Néel relaxation time* [6] [7] (see equation 2.8). When a magnetic field is not present, and the time one takes to make the measurement of the magnetization is longer than this relaxation time, the magnetization will appear to be zero, in average. The particle is said to be in a *superparamagnetic state* [8]. In this state, the particles are magnetizable with the use of a magnetic field and stay magnetized only on the presence of the field, as happens with paramagnetic materials. In fact, the superparamagnetic particles have a much larger magnetic susceptibility which means that their magnetization is higher than that of typical paramagnetic materials. When the particles remain magnetized

after the removal of the field they are said to be in the *blocked state*. The temperature at which this happens is called the *blocking temperature* [9]. As our work is always made at room temperature, the concept of a changing blocking temperature is to us not important.

2.4.1 Hysteresis Loop

A hysteresis loop, as the one shown in figure 2.3, gives us the relation between the magnetization and the magnetizing field of a magnetic material. A ferromagnetic material that has no magnetization will increase its magnetization along the dashed green line with increasing magnetizing field until it reaches saturation, M_{sat}, when all the magnetic domains are aligned to the field. Reducing the field to zero, going along the upper blue line, we will see a reduction of the material's magnetization. The point where it intersects the vertical axis, M_{rem}, is called remanent magnetization and gives us the quantity of magnetization that remains on the material. This happens because some magnetic domains still remain aligned, even though the magnetizing field H is now zero. Continuing along the upper blue line, we reach the point where it intersects the horizontal axis, H_{coe}. This point gives us the coercive field, which is the field required to remove all remanent magnetization and it means that now all magnetic domains add up to zero. The process continues until a new saturation point is reached, this time with the magnetizing field in the opposite direction. Increasing once again the field H, we will have a similar line shifted to the right until the loop is closed at the first saturation point.

Still looking at the same figure, we can see a red line. This is the line that describes the behavior of a superparamagnetic material, in our study, nanoparticles. As we can see clearly, there is no hysteresis in its behavior. The remanent magnetization is zero and so is the coercive field. The inclination of the curve, gives its magnetic susceptibility. As seen in the figure, the superparamagnetic particles have a higher magnetic susceptibility [10].
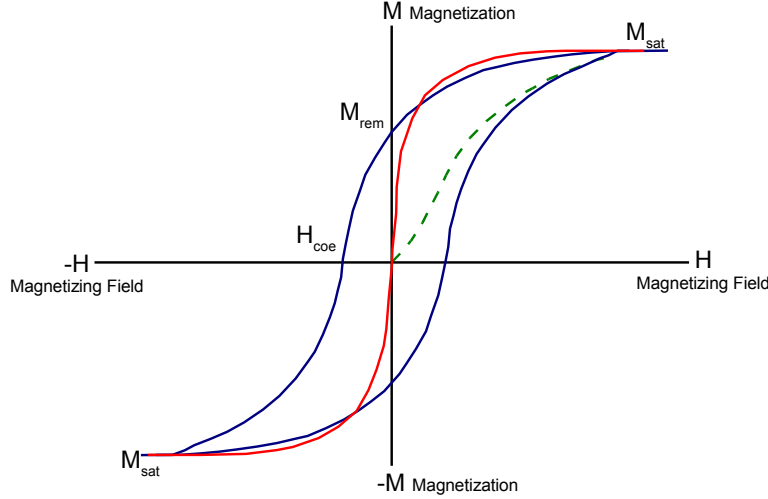
Figure 2.3: In green and blue the hysteresis loop of the magnetization of ferromagnetic microparticles due to the presence of a magnetic field B. In red the magnetization 'loop' of a superparamagnetic nanoparticle.

2.4.2 Néel relaxation time

Bulk ferromagnetic material is in the paramagnetic state when its temperature is above Curie Temperature (T_c)[1] [11]. The difference to our superparamagnetic particles is that the paramagnetic state is reached at a temperature orders of magnitude below the Curie temperature of the constituent material. As shown in equation 2.7 that describes the Curie Law,

$$\mathbf{M} = \chi \cdot \mathbf{H} = C \cdot \frac{\mathbf{H}}{T}, \tag{2.7}$$

(with $\mathbf{M}$ the resulting magnetization, χ the magnetic susceptibility, $\mathbf{H}$ the magnetizing field, T the absolute temperature and C the material-specific Curie constant) the magnetization of a paramagnetic material is proportional to the applied field and inversely proportional to the temperature. This also means that the magnetic susceptibility χ of the particles is inversely proportional to the temperature T.

This happens with superparamagnetic nanoparticles because they are small enough to be described by, what is called, a *macro-spin approximation* which means that all the

---

[1]Typical ferromagnetic materials as iron, nickel, cobalt have $T_c = \sim 1000\ K$
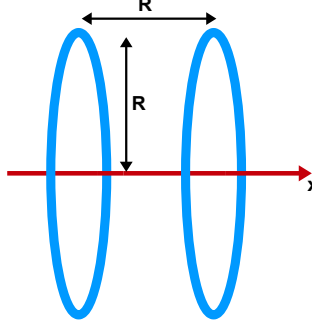
Figure 2.4: Example of a Helmholtz coil. The distance between coils must be the same as the coils' radius.

individual magnetic moments carried by the atoms of the nanoparticle can be considered as a single magnetic moment [12]. In a simple approximation, we can assume an uniaxial magnetic anisotropy, i.e. the free energy of the particles is lowest for the magnetic moment being orientated along one axis. Both orientations are separated by the energy barrier KV mentioned in equation 2.8. At temperature above absolute zero, the magnetization is not fixed in one direction due to the thermal excitation.

The mean time between two changes in direction is as previously said, the *Néel relaxation time*:

$$\tau_N = \tau_0 \exp\left(\frac{KV}{k_B T}\right) \tag{2.8}$$

where τ_0 is the attempt time [13], characteristic of the material and typically 10^{-9} to 10^{-10} s, K is the magnetic anisotropy energy density of the particle with V the volume of the particle. The product KV is the energy barrier the magnetic dipole has to overcome in order to switch to the opposite direction. The probability for this switch to happen depends on the ratio between this energy and the thermal energy $k_B T$, where k_B is the Boltzmann constant and T is the temperature.

2.5   Helmholtz Coil

Invented by Hermann von Helmholtz in the middle of the 19th century, the Helmholtz coil is a device that produces nearly uniform magnetic fields. It is composed of two circular coils that are positioned parallel to one another at a distance equal to the radius

Name	Size (µm)	Surface	Type	Company
Dynabead MyOne	1,0	Streptavidin	PMMA with distributed iron nanoparticles	Invitrogen
Dynabead 27	2,7	Streptadivin	PMMA with distributed iron nanoparticles	Invitrogen
Dynabead 28	2,8	Carboxyl	PMMA with distributed iron nanoparticles	Invitrogen
Epoxy	1,0	Epoxy	Silica with 60% nucleus of iron	Bioclone
PS-MAG	11,0	N/A	PS with distributed iron nanoparticles	MicroParticles

Figure 2.5: Various types of beads and their characteristics.

of each one and that share the same central axis (see figure 2.4). This device produces a magnetic field composed of parallel lines at the center of the apparatus when current flows inside the wires that compose the coil (see right side of figure 2.1). The direction of the magnetic field can be predicted using the right-hand rule and the magnetic field's intensity is calculated at the center using a derivation of the Biot-Savart law [15]:

$$B = \left(\frac{4}{5}\right)^{3/2} \frac{\mu_0 n I}{R} \tag{2.9}$$

where μ_0 is the permeability constant in vacuum, n is the number of turns of the wire, I is the current and R is the radius of the coils.

In this work, we use two almost-Helmholtz coils (meaning four coils, see figures 3.2 and 3.3 on page 23) that are disposed at 90° relative to one another, being the plane composed by the intersection of the two axis horizontal. In order to achieve this, one of the pairs has to be smaller than the other, because of the restriction that the distance between coils must be equal to the radius. We call them almost-Helmholtz coils due do the fact that their distance does not obey this restriction as we will see later.

2.6 Magnetic Microparticles

In our work we used a small variety of different micro sized superparamagnetic particles, usually called *Magnetic Beads* (in this work, they will loosely be called beads). Varying in size, function and quality. The table in figure 2.5 shows their names, companies and some characteristics and figure 2.6 shows the two different types of magnetic material distribution.
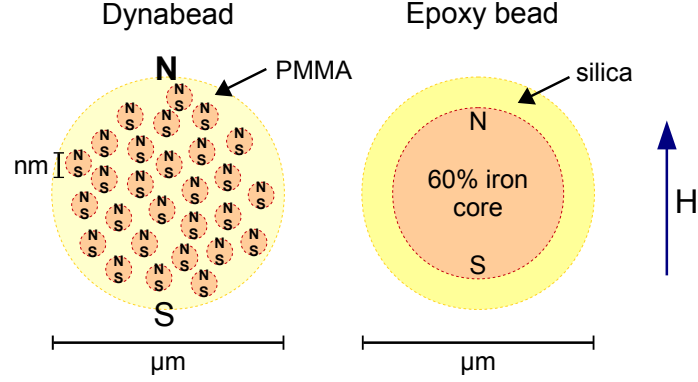
Figure 2.6: The two types of beads. On the left the PMMA Invitrogen Dynabeads with evenly distributed iron nanoparticles (26% of the mass) and on the right the Bioclon silica Epoxy activated magnetic beads with a 60% iron core.

2.6.1   Characteristic and Types

The uses of magnetic beads on the market are very oriented on the rapid separation and isolation of cells and DNA strands [22].

Some examples of uses taken from the website of one of the companies that manufactures these beads, Invitrogen, are Cell Separation, Protein Isolation, Nucleic Acid Isolation and mRNA isolation in 15 minutes, among others. The aim of use of this particles does not require the study of their magnetic properties and physical characteristics and so, magnetization values, susceptibility, even mass and iron content is data not given by the companies, and could only be found in specific scientific papers, many of them included in the bibliography. [1] [2] [5]

As we can see in the table, we have two different types of beads (check figures 2.5 and 2.6).

The Dynabeads MyOne, 27 and 28, beads from the company Invitrogen[1], and the PS-MAG-S2392 11 μm fluorescence beads from MicroParticles[2], which are beads made of PMMA (Poly(methyl methacrylate)) (Dynabeads) or Polystyrene (PS-MAG) with an uniform distribution of iron nanoparticles which are superparamagnetic. And then we have the Bioclone's[3] Epoxy activated beads which are constituted by an iron microcore

---

[1]http://invitrogen.com

[2]http://microparticles.de

[3]http://bioclon.com
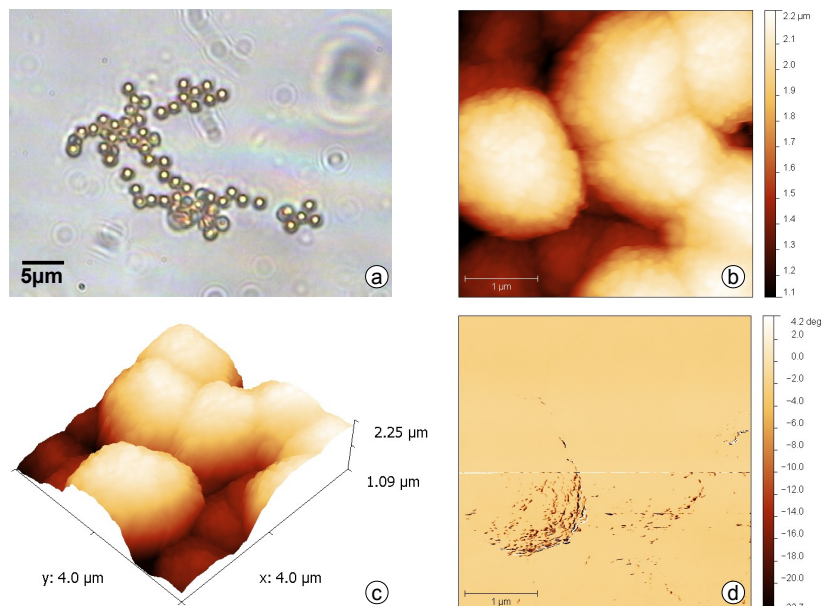
Figure 2.7: Various microscopies of the 1.0 *μm* Dynabeads: (a) Optical microscopy (100x), (b) Atomic force microscopy, (c) 3D modulation of the AFM, (d) Magnetic force microscopy.

covered by silica.

After some experiments were made with both types of coils a doubt emerged. Are the beads bought really superparamagnetic or not. The experiments with the Dynabeads showed no signs of false superparamagnetism, they would very rapidly be influenced by the Brownian motion [16] and spread apart. It was the experiments with the Epoxy beads that lead to some confusion and doubt. These would remain stuck to each other even after a long time with no magnetic field present. Trying to test this with our system was difficult and it was at an early stage attributed to the activated epoxy on the surface, even though the calculations lead to believe they were not superparamagnetic at all. The results are very clear, while the Néel relaxation times for the Dynabeads resulted in 14 *ns*, the calculated time it took for the Epoxy beads to relax would sum up to more than the age of the Universe.

To solve this mystery two Atomic Force Microscopy and Magnetic Force Microscopy experiments were made involving the beads. The samples used for both microscopies where dried beads, previously used in experiments, on the surface of glass plates without
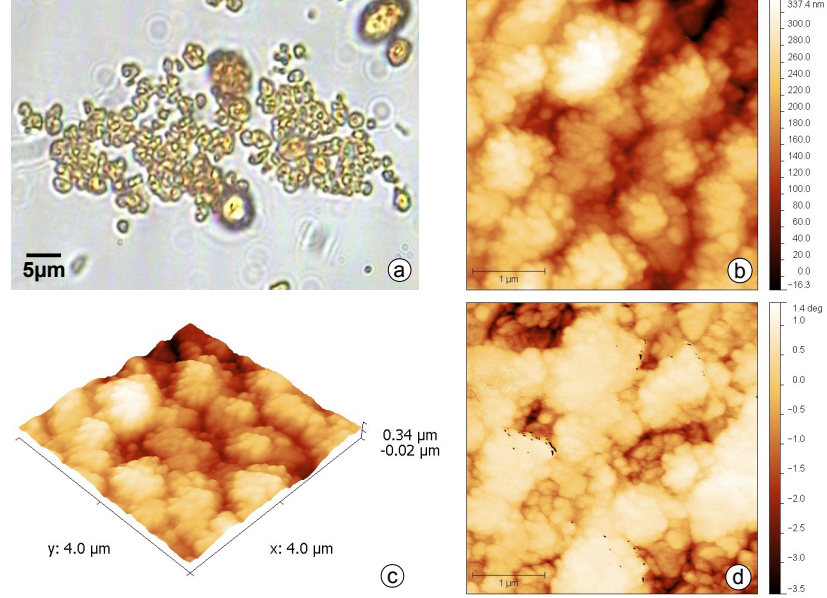
Figure 2.8: Various microscopies of the Epoxy beads: (a) Optical microscopy (100x), (b) Atomic force microscopy, (c) 3D modulation of the AFM, (d) Magnetic force microscopy.

the presence of any magnetic field, other than the one produced by the magnetized cantilever tip of the AFM (see figures 2.7.a and 2.8.a). On the same figures we are able to see the AFM and a 3D modulation, made from the height data obtained with the AFM (figure 2.7.b and 2.7.c and 2.8.b and 2.8.c). The MFM data represents the shift in resonance frequency of the cantilever excited at fixed distance of 80 nm above the surface (figures 2.7.d and 2.8.d).

Comparing both particles, we see that the Dynabeads present a much more round and uniform shape than the Epoxy beads. But this is also visible in the Optical microscopy and is not new information. What is interesting to see is presented at the (d) part of both figures. On the figure of the Dynabeads we see that no magnetic dipole moments are present. The darker zones of the graph show us where the needle touched the particles and not a difference in phase due to the presence of a magnetic field. This is explained by the fact that they are superparamagnetic. The magnetic dipole moment follows the needles magnetic field and so the needle suffers no disturbance in the phase. As we glance now to the results from the Epoxy beads, the story is a bit different. As clearly seen in figure 2.8.d, these present strong magnetization, long time after
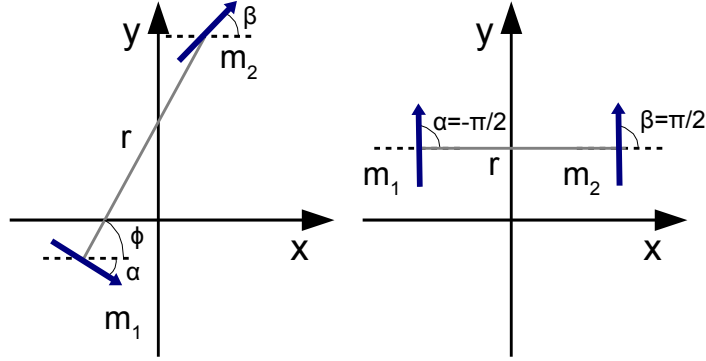
Figure 2.9: On the left the global coordinates system used in equation 2.11. On the right the position of the parallel dipole moments as calculated in figure 2.10.

they were in the presence of the magnetic field generated by the coils. The phase of the needle is changed, reduced and increased, which reveals the presence of magnetic dipole moments in various directions.

This discovery helped us to understand the behavior of the Epoxy beads and makes us feel a bit fooled by the company, which has sold them as superparamagnetic.

2.6.2 Forces on Magnetic Beads

2.6.2.1 Magnetic Force

The magnetic dipole moment [17] of a particle is calculated with as shown in equation 2.10:

$$\mathbf{m} = \mathbf{H}\mu_p M_p. \tag{2.10}$$

with $\mathbf{H}$ the magnetizing field applied, M_p the particle's mass and μ_p its magnetic mass susceptibility.

The forces between two magnetic dipoles can be calculated using equation 2.11 [17] (for a visual help refer to figure 2.9):

$$F_r(r,\alpha,\beta) = -\frac{3\mu_0}{4\pi}\frac{m_1 m_2}{r^4}\left[2\cos(\phi-\alpha)\cos(\phi-\beta) - \sin(\phi-\alpha)\sin(\phi-\beta)\right] \tag{2.11}$$
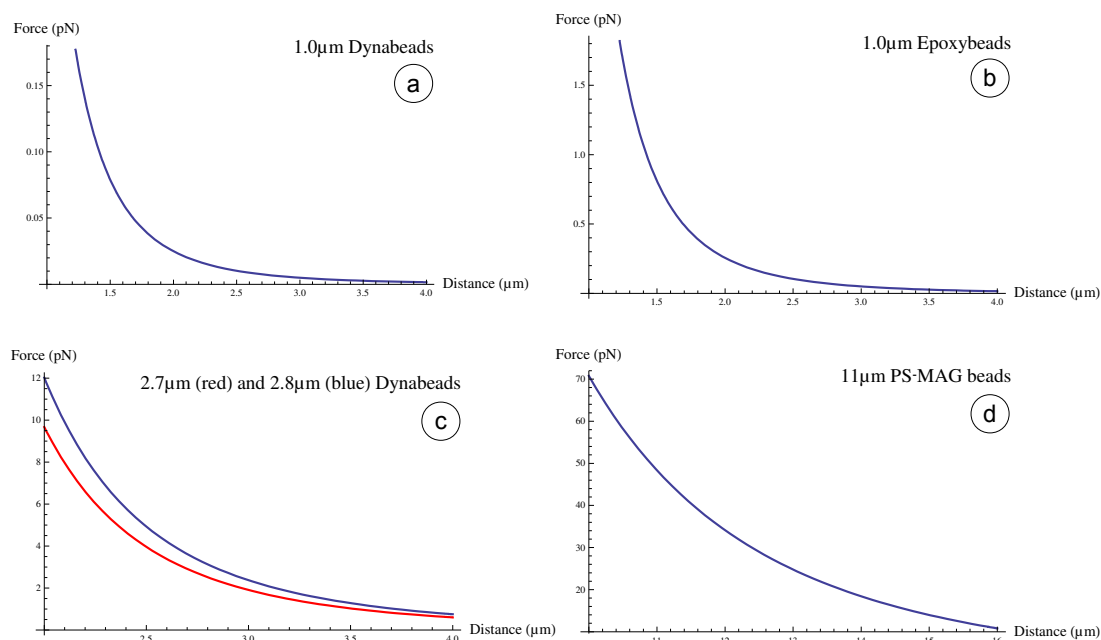
Figure 2.10: Absolute values calculated for the force between two beads of various diameters composed of a micrometer plastic container with scattered nanoparticles (a), (c) and (d) and a bead with a 60% ferrite microcore (b), with parallel dipole moments generated by an 18 mT magnetic field.

Bacteria-Antibody bond   DNA unzipping
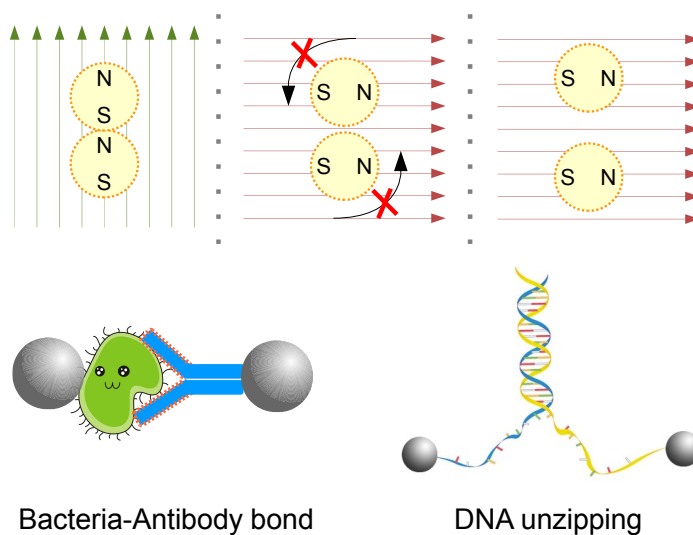
Figure 2.11: Behavior of superparamagnetic particles in a changing magnetic field. On the bottom the idea of the work, to control and manipulate macromolecules and cells.

where F_r is the force between the two magnetic dipoles m_1 and m_2, r is the distance between the centers of both dipoles, ϕ is the angle between the X axis and the line that connects centers of both dipoles, α the angle between $\mathbf{m}_1$ and the X axis and β the angle between $\mathbf{m}_2$ and the X axis.

On our work we calculated the force between the various types of magnetic particles when the dipole moments are parallel to one another (see figure 2.9). The results are presented in figure 2.10. These calculations are made in order to understand the behavior of the particles in a changing magnetic field. This idea is schematized in figure 2.11.

As is visible in figure 2.10, the force resulting from the interaction between two magnetic dipoles strongly depends on the distance between the dipoles and on the size of the particles. To calculate these forces we had to do some approximations. One of them was to assume that the sum of all dipole moments of the nanoparticles of the Dynabeads (see left part of figure 2.6) is the dipole moment of the microparticle [12]. Another approximation was to assume that the particles are perfect spheres and the dipole moment is reduced by 1/3 due to the demagnetizing field [12].

2.6.2.2   Gravity Force

Although not very relevant to our work, due to it being perpendicular to the plane of work, the magnetic particles are also acted by the ever present gravitational force [15] (see equation 2.12).

$$\mathbf{F_g} = -m_b g \mathbf{e_z} \tag{2.12}$$

where $\mathbf{F}_g$ is the force exerted on the particle, m_b is the buoyant mass of the particle ($m_b = V(\rho - \rho_f)$, with V the volume of the particle, and ρ and ρ_f the densities of the particle and the surrounding fluid respectively), g is the gravitation constant and $\mathbf{e_z}$ the Z axis direction.

As an example of calculation [5], we take the Dynabead MyOne 1.0 μm diameter particle, which has a volume of 0.52 μm^3, 26% iron content and a density of 1.8 g/cm^3, in water which results in a gravitational force of 0.004 pN which is smaller than the force generated by the coils.

2.6.3 Behavior in the Presence of a Magnetic Field

Due to the formation of the stray magnetic induction of the particles (figure 2.6), these will interact with each other, forming chains and sheets (see right side of figure 2.2 and figure 4.7). The idea (see figure 2.11) is to use this stray magnetic field to spread two particles apart. By changing the magnetic field by 90°, the magnetization will also rotate 90° and the once co-linear dipole moments will now be parallel, provoking a separation of the particles. This, the change of field and consequent change of direction by the dipole moments, has to occur in a time scale smaller than the time it takes for the particles to rotate to accommodate to the magnetic induction. The graphics in figure 2.10 show the various values of forces that can be used with this technique.

When the rotation of the magnetic field is small, the particles will have time to adjust to the new field and the columns, and/or sheets, will then rotate together. These characteristics of the behavior of the particles permitted the development of various operation modes shown and explained in section 3.3.

2.7 Conclusion

In this chapter we began by explaining the physical concepts required for the understanding of the behavior of the superparamagnetic microparticles in the presence of the dynamic magnetic fields: electromagnetic fields, magnetic moment, superparamagnetism, hysteresis, Néel relaxation times and Helmholtz coils. We introduced the different types of superparamagnetic microparticles used and calculated their interacting magnetic forces. Some study on the characteristics of the superparamagnetic microparticles was also made in order to understand strange phenomena, namely the non-superparamagnetic behavior of the Epoxy beads.

3

Design of the System

The main aim of this work is the design and construction of a system that can control superparamagnetic microparticles. This was accomplished with two pairs of Helmholtz coils disposed in a perpendicular way (figure 3.3). To begin the project we had to check what equipment and material was available for our use. To our misfortune, one of the power supplies was broken. We ended up having a 30 V, 10 A linear power source, Statron Typ 3203, to supply all the power to the coils and to the controlling circuit instead of a high-voltage power supply capable of amplifying signals of higher frequency. Because of this the design of the coils was changed from, thousands of turns and consequently high resistance (200 Ω) and voltage (200 V), to hundreds of turns with thicker wires, which provided coils of low resistance (10 Ω) and so low voltages (30 V) could be applied, with the inconvenience of the need of the use of high current, 3 A, which originated problems in the rapid change of direction of the magnetic field and heating of the system.

In this section we describe in detail the characteristics, functionality and limitations of the system.
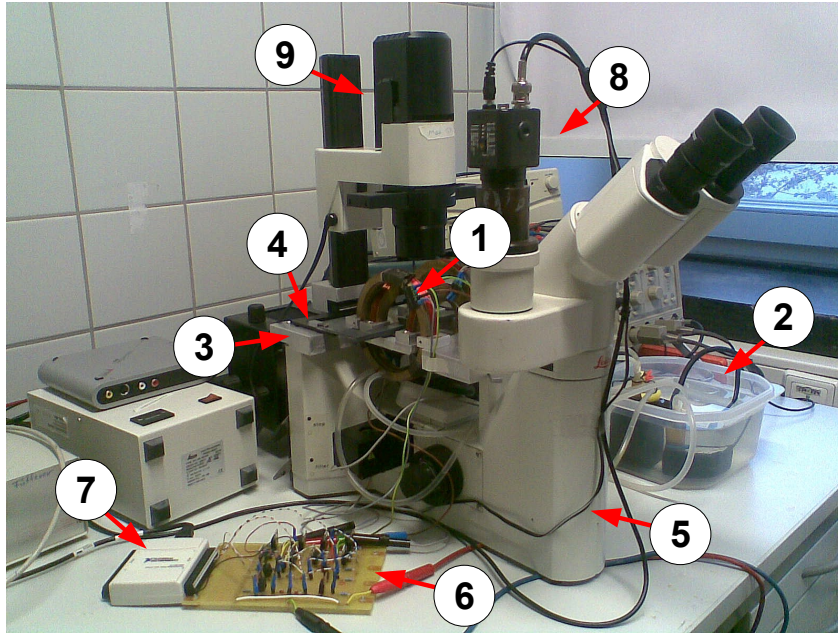
Figure 3.1: Overall view of the system and working desk: (1) Two Helmholtz coils, (2) Cooling system, (3) Supporting table, (4) Moving table and Sample holder, (5) Microscope, (6) Electronic controlling circuit, (7) Computerized control (NI USB-6008 DAQ), (8) Video camera, (9) Lighting system.

3.1 Structure and Specifications

Beginning by the structure of the system, we show its different functional parts (refer numbers to figure 3.1):

1. Two Helmholtz coils

2. Cooling system

3. Supporting table

4. Moving table and sample holder

5. Microscope

6. Electronic controlling circuit

7. Computerized control (NI USB-6008 DAQ)

8. Video camera
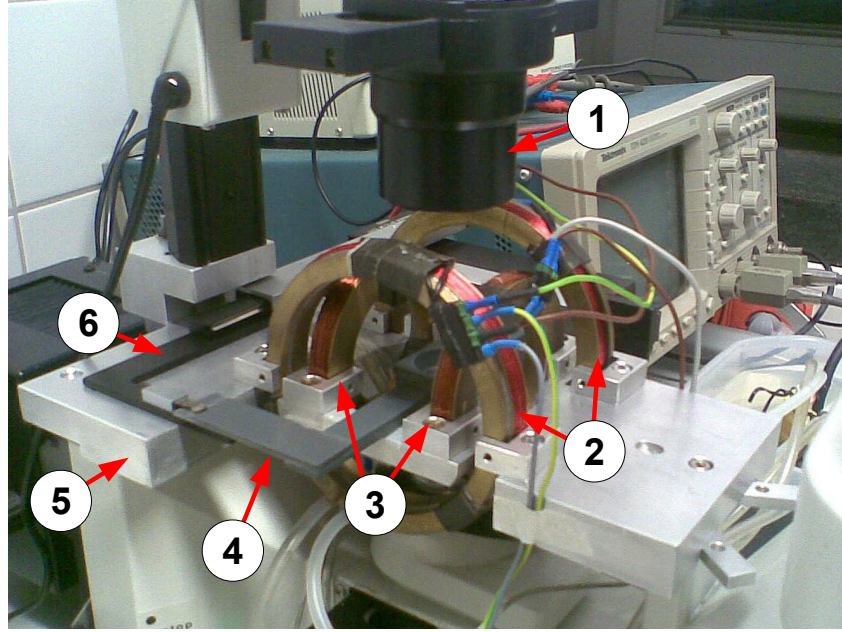
9. Lighting system

Figure 3.2: Close view of the coils and microscope: (1) Lighting system, (2) Big coils, (3) Small coils, (4) Sample holder, (5) Microscope table, (6) Moving table.
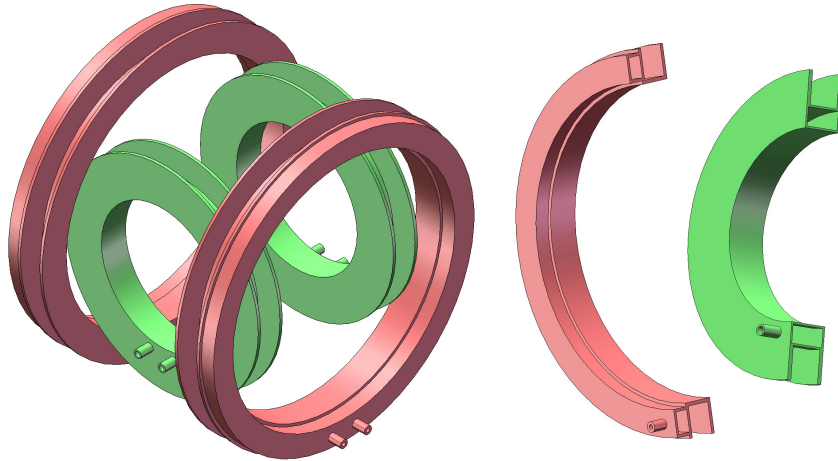
Figure 3.3: On the left two pairs of Helmholtz coils. The difference in size permits the coils to be approximately at the correct distance. On the right a cut-view to show the cooling chambers.

	Small coil	Big coil	
Turns	300	320	
Radius	3,5	5,0	**cm**
Resistance	10,5	11,0	**Ω**
Inductance	8,7	18,7	**mH**
Power dissipated	94,5	99,0	**W**
Magnetic Field (single)	14,1	10,0	**mT**
Magnetic Field (pair)	18,2	12,3	**mT**

Figure 3.4: Specifications of both coils.

The mechanical design of the system was made having several aspects in mind. One of the most crucial and the one that dictated all others was the space available. Having to use a small microscope, all the design had to manage to create a system with the desired characteristics, suitable field intensity, minimum heat problems, focusing space for the objective and most importantly space for a sample to be maneuvered. On top of the design problems we had also construction problems originated on the difficulty in constructing the coils, winding the wire and finally mounting them tight.

The Helmholtz coils (close view in figure 3.2 and 3.3 and technical details in figure 3.4) were designed by us and constructed and soldered in the Workshop of the Physics Faculty of the University of Leipzig and are made out of tin (case) and copper (wiring). As can be seen in figure 3.3 the cooling chambers are different for each coil. This is due to space restrictions. The cooling chamber of the Small coil (represented in green) is below the coiled cable chamber and has a volume of 8 cm^3. The cooling chamber of the Big coil is situated at the outer side of the coil with a volume of 9 cm^3. This proved to be insufficient to effectively cool down the coils as we latter discuss. The most difficult part on the construction of the coils was to effectively water tight the cooling chambers. This tightening would be broken after the winding and sometimes after the simple mounting on the microscope.

The cooling system is composed by two off-the-shelf waterpumps (see figure 3.6), and a plastic open container as a cold water deposit. The water flows in a closed-circuit and is refrigerated only by the room temperature air at the surface of the open container.

The supporting table was specifically designed for this experiment and had to employ the four coils, the moving table and the lighting system as well as not disturb the focusing and lens system (close view in figure 3.2). It was also made by the Workshop

Variation of magnetic field with temperature of coils
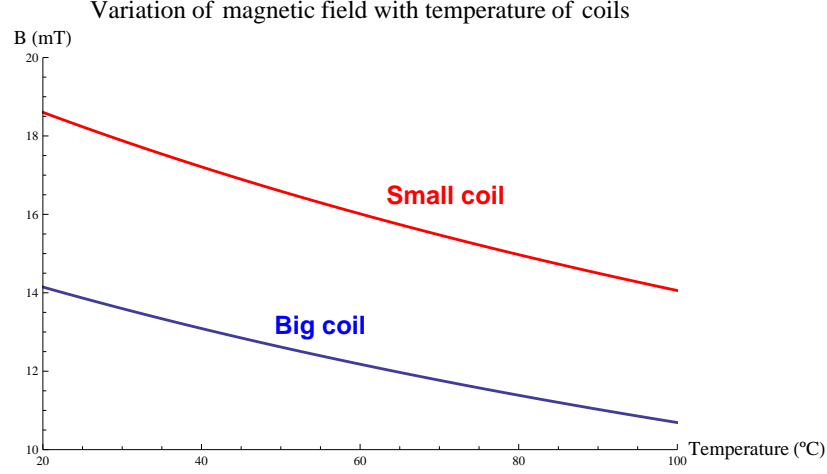
Figure 3.5: Calculation of the variation of magnetic field with increase of temperature.

and is made out of aluminium.

An already existent precision moving table was changed to fit our purposes (again a better view in figure 3.2). A new sample holder had to be designed in order to move the sample in the tight space available between the coils. The sample holder is made out of PMMA to avoid interference with the magnetic field. This method of moving the sample permits us to have it always at the center of the generated field, which is the area where it is most uniform.

The electronic controlling circuit was designed and built by us. It employs four voltage converters and two half-bridge circuits (as seen in figures 3.9 and 3.10).

The computerized control is made using an electronic device from National Instruments, NI USB-6008, that is controlled by LabVIEW on a regular PC (Personal Computer) via USB (Universal Serial Bus).

3.1.1 Energy Consumption and Generated Heat

The resistance of the coils increases with the temperature, making the magnetic field's intensity lower (figure 3.5). To check if a cooling system was required some calculations on power of the coils and their heating were made. At the beginning we thought that two fountain waterpumps (figure 3.6) flowing room temperature water through a closed circuit would be enough. At the end we saw that the cooling system is not perfect as it does not completely cool the pumps. To try and solve the problem ice 'crumbles' may

25
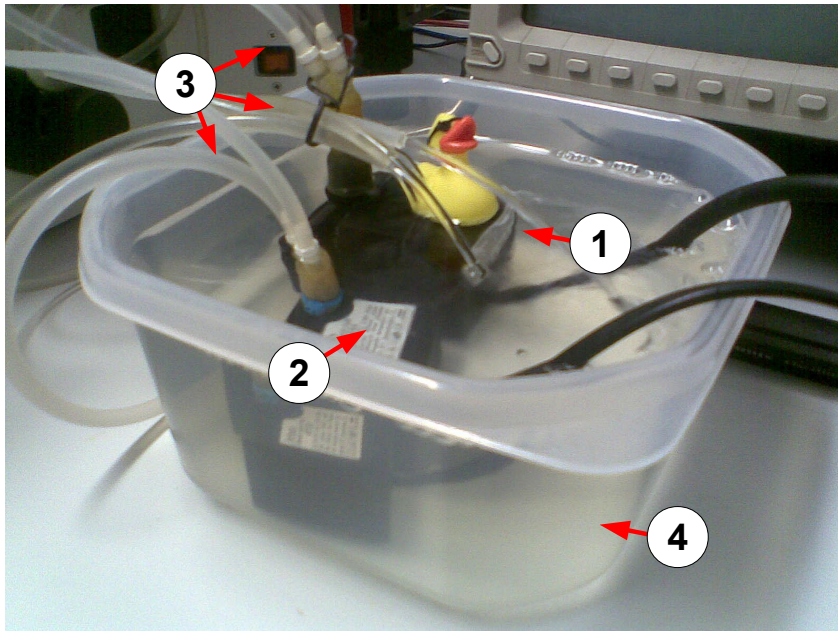
Figure 3.6: Close view of the cooling system: (1) Big pump, (2) Small pump, (3) Tubes connecting to cooling chambers, (4) Water deposit.

be added to the water deposit. This presents itself as a temporary solution as the ice rapidly dissolves. The power dissipated by each coil is, $P = RI^2 = 10.5 * (3)^2 = 94.5$ W for the small coil and $P = RI^2 = 11 * (3)^2 = 99$ W for the big coil (table in figure 3.4), and the calculated amount of room temperature water flux necessary for cooling is then, 60 g/s for the small coil and 134 g/s for the big coil. The fountain waterpumps deliver water with a much lower flux than the one publicized, at a rate of 6 g/s and 12 g/s respectively for cooling the small and big coil against the 80 g/s and 120 g/s specified in the manuals. This lower flux is due to the higher pressure they find in the cooling chambers.

3.1.2 Magnetic Field Generation and Uniformity

For the magnetic field generation a simulation was also made (figure 3.7). As the mechanical design obliged us to spread the coils apart more than is usual on a typical Helmholtz coil, the generated magnetic field's intensity was diminished. The problem we encountered has to do with the space available and disposition of the lenses and focusing system on the microscope used. The small coils (green in figure 3.3) are
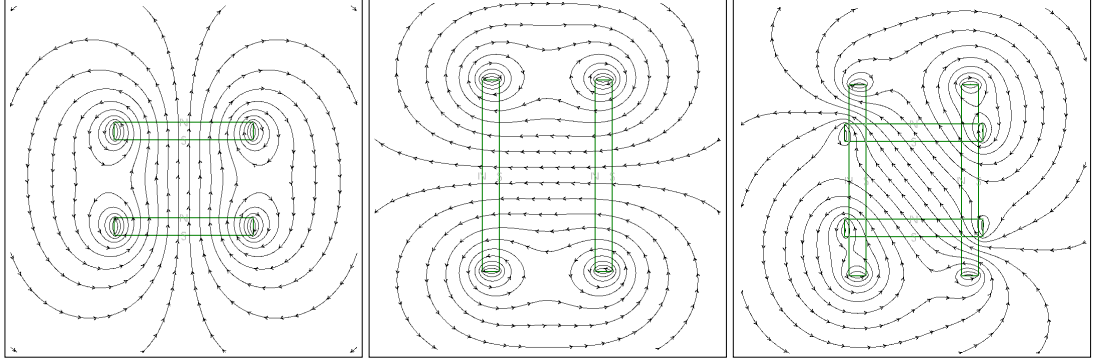
Figure 3.7: View top of a simulation of the magnetic field produced on a plane parallel to the page which contains the coils' center axes.
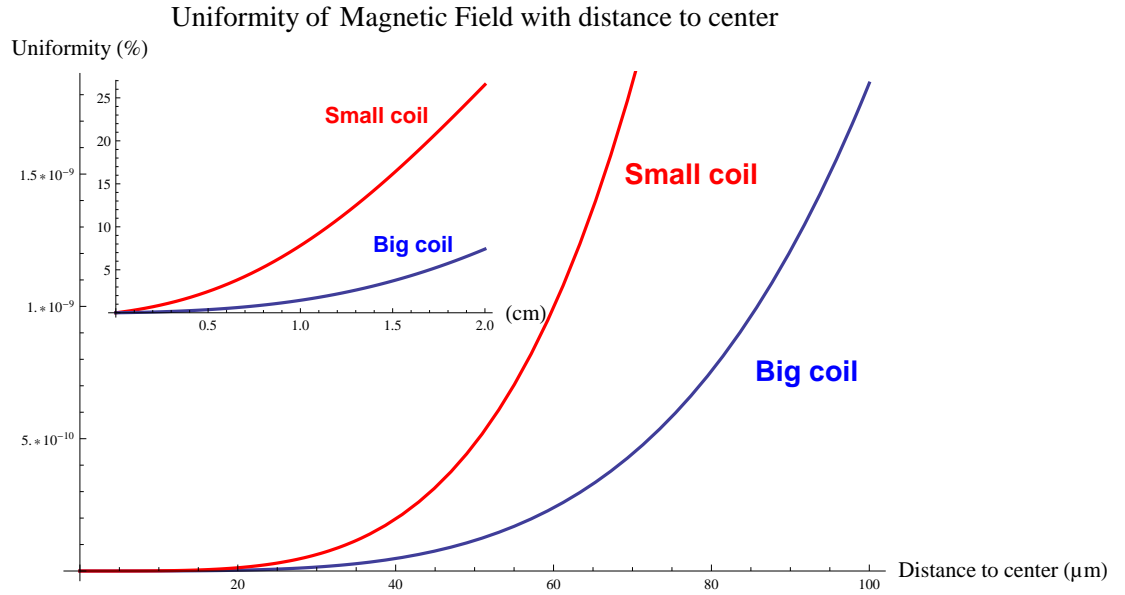
Figure 3.8: Uniformity of the magnetic field produced by the Small and Big Helmholtz coils. The area used for the study is that of a square with no more than 100 μm of side which presents a very uniform field.

actually 5 *cm* apart instead of the theoretical 3.5 *cm* and the big coils (red in figure 3.3) are 6.5 *cm* apart instead of 5 *cm*. This reduces the intensity of the field produced and the area of uniformity, but, as shown in section 3.1.2 in page 26, the uniformity of the work area is maintained. On the left part of figure 3.7 the simulated coils have the dimensions of 8 per 1 *cm*, are 5 *cm* apart, contain 300 windings of wire and a current of 6 *A* is used (for each pair). It represents the small coils, drawn in red in figure 3.3. The simulated value of the magnetic field B is 19 *mT* (the real measured value is 18 *mT* $\pm 5\%$)[1] at the center. The center part of the figure shows coils with dimensions 1 per 11 *cm*, 6.5 *cm* apart and 320 windings with the same current, they represent the big coils, drawn in green in figure 3.3. The value of the magnetic field is calculated to be 14 *mT* (real 12 *mT* $\pm 5\%$) at the center. The figure on the right represents the magnetic field produced when both coils are turned on, the magnetic fields intensity is 22 *mT* (real 18 *mT* $\pm 5\%$ due to 10 *A* current limitation of the power source). These simulated values are not exactly equal to the ones measured experimentally, mostly due to imperfections on the coils' fabrication: twisted wires because of the fact that the coils are not made of only one wire, the fact that the other coils are always present even if turned off, and a possible misalignment of the pairs of coils. This difference can also originate on the misaligned position of the Gaussmeter probe.

Added to the simulation of the magnetic field's intensity, a simulation on the uniformity of the field was also made. Figure 3.8 shows that the field is extremely uniform and more than enough for the area in which the experiments are made.

3.2 Control

The control of the system is made with the help of an electronic circuit which is controlled by an electronic device, namely a NI USB-6008 DAQ from National Instruments (figure 3.9, white box on the left), that is by its turn controlled by LabVIEW software. We will explain the electronic circuit and electronic device and the reasons why they were chosen, but first a quick look at the time characteristics of the system.

---

[1]The magnetic field's intensity was measured using a calibrated Gaussmeter with a 5% accuracy.
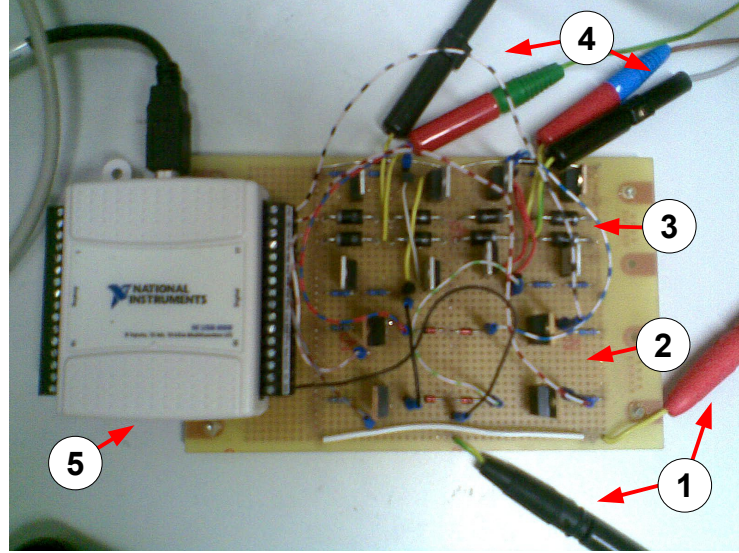
Figure 3.9: Electronic circuit that controls the current delivered to the coils: (1) Power cables, (2) Four converter circuits, (3) Two Half-Bridge circuits, (4) Connections to the coils, (5) NI USB-6008 controller.

3.2.1 Relaxation Times

The inductance of the coils delay the disappearance of the self-induced voltage due to the sudden cut of the flow of current through the MOSFETs. In figure 3.11, we find the simulated relaxation times, (a), and the actual measured times, (b) and (c), for both coils. The relaxation times were simulated for coils with 10 Ω and 9 mH for the small coils and 11 Ω and 19 mH for the big coils. The difference between the simulated, 0.9 and 1.53 ms, and the measured times, 1.0 and 1.50 ms is acceptable. This relaxation time implicates the slow disappearance of the magnetic field which causes the magnetic dipoles of the particles to rotate instead of jumping when the field is changed by 90°. The wave forms are also different. On the simulated values, we see a ripple which is not present on the measured signals.

3.2.2 Electronics

Connected to a PC is the NI USB-6008 controller from which four digital outputs are used. These outputs control an electronic circuit which then controls the current supplied to the coils. The electronic circuit was extensively simulated before its assembly.
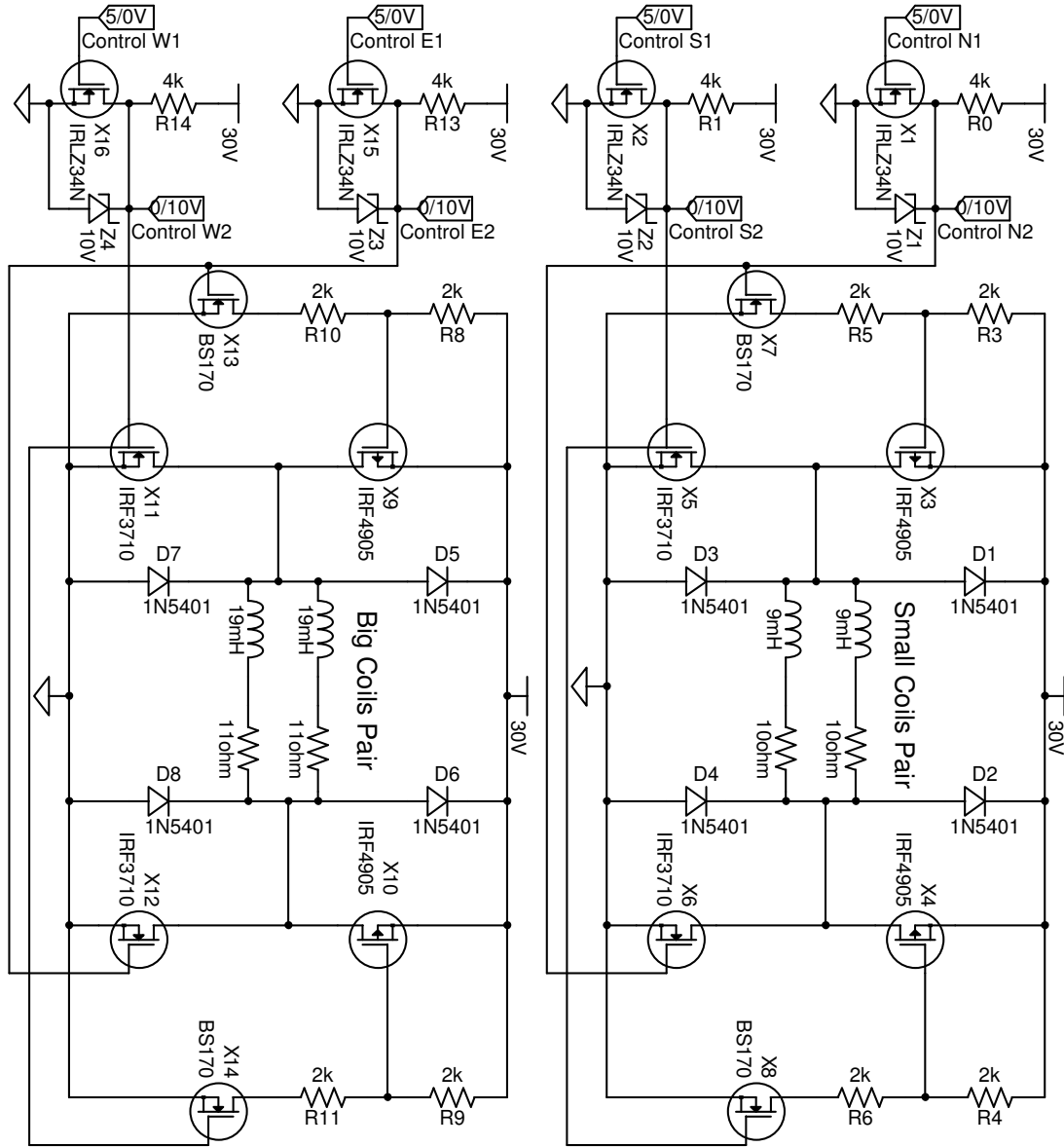
Figure 3.10: Four $5 - 0\ V$ to $0 - 10\ V$ converters and two Half-Bridges. Each one of the Half-Bridge circuits control one pair of coils shown in the middle as the parallel of a series of an inductor and a resistance.
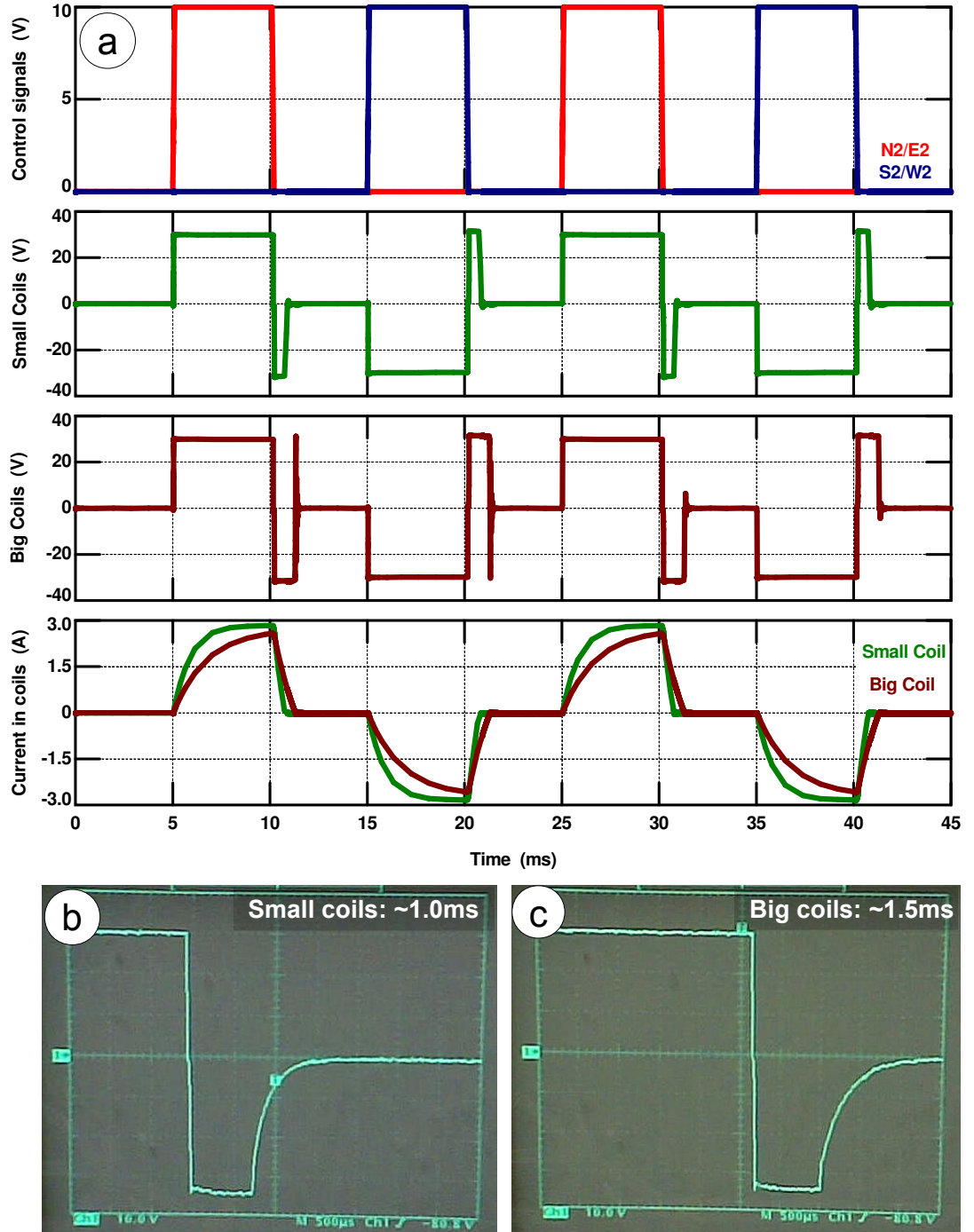
Figure 3.11: (a) The graphic on top shows the variation of the control signals of both coils, Control N2/E2 and S2/W2 signals. The second and third graphics show the voltage variation on the small and big coils. The fourth graphic shows the variation of current on one of the small and big coils. Note the self-inducted voltage when the voltage is brought back to zero at both coil pairs. The measured relaxation times for the small (b) and big coils (c) are also presented.

The simulation circuit can be seen on figure 3.10 which we will use to explain its function. On the top left corner of the figure we have on of the voltage converters. This is used to convert the $5 - 0\ V$ (for example, Control N1) signal coming from the NI USB-6008 to $0 - 10\ V$ (for example, Control N2) that are necessary to open the MOS-FETs. This is made with the help of the Z1 10 V zener diode and the X1 IRLZ34N MOSFET. At the gate of the X1 MOSFET we have the signal (Control N1) provenient from the NI USB-6008 controller. This signal is maintained at 5 V when the system is in standby. At 5 V we have a flow of current through the opened X1 MOSFET. This way, the 30 V fall at the 4 $k\Omega$ resistor and at the upper part of the Z1 zener diode we have 0.7 V (not enough to open the MOSFETs). This voltage maintains the gate at the X7 BS170 and the X6 IRF3710 closed (Control N2 in this case, but the same applies to all other Control signals). When the signal at Control N1 goes to 0 V, the X1 IRFZ34N MOSFET is closed and at the Z1 zener diode we have then a fixed 10 V voltage (Control N2) (refer to figure 3.10, upper part). The left transistor X7 BS170, and the bottom right transistor X6 IRF3710, will open. Being a p-type channel MOSFET, the X3 IRF4905 will open when a voltage inferior to $-10\ V$ is established between the gate and the drain. With the use of a voltage divider (with 2 $k\Omega$ resistors R3 and R5), a voltage of $-15\ V$ (15 V - 30 V) is obtained, and so the transistor conducts in the saturation zone. We have then the flow of current in a specific direction through the coils, here represented by a series of a 10/11 Ω resistor and a 9/19 mH inductor (for small/big coil). To change the flow of current to the other direction (still at figure 3.10 upper part), the Control S1 signal, correspondent to the Control S2 will have to go to 0 V and the same will happen as before. These two pairs of signals, Control N2 and S2 or Control E2 and W2, may never be at 10 V at the same time, or else we will have a short circuit. The diodes D1-D8 are an important part of the circuit as they allow the discharge of the coils when the flow of current is halted. To have an idea of the real circuit one can glance at figure 3.9.

On the figure 3.11 we have the simulated transient analysis of the signal made with the TopSPICE simulator program[1]. The graphic on top shows the variation of the Control N2/E2 and S2/W2 signals. On the second and third graphics we can see the voltage applied to the small coils and big coils respectively, varying from 0 V to 30 V or -30

---

[1]http://www.penzar.com/topspice/topspice.htm

V depending on the direction of the current. Both figures show a self-inducted voltage that occurs when the current is halted. This occurs because of the electromotive force on the coil produced by the changing magnetic field that tries to counteract the change in current. As said before, this self-inducted voltage slows down the effective disappearance of the fields. This has its consequences on the proper separation of the beads as shown in the *Results and Experiments* chapter. The simulated signal differs from the measured signal in that the first one shows signs of oscillation not present on the measurement with the oscilloscope. This oscillation may derive from an artifact in the simulation engine of the software. Nonetheless the signals are very similar. When the control signals change from 10 V to 0 V at times 10, 20, 30 and 40 ms, both show a sudden decrease from 30 V to -30 V which is maintained for a period of time and then increases with an exponential form to zero. This happens because the current that flows through the coils is suddenly halted and a self-inducted voltage is created by the response of the coils to this change in current. The current flows then to the power supply with the help of the diodes D1-D8 with a relaxation time dependent on the inductance and resistance of the coils and the power source, $\tau = L/R$. The bottom graphic on figure 3.11 shows the variation in current. The frequency of the control signals used in the simulation is the highest possible output frequency for the NI USB-6008 DAQ, 200 Hz. We see clearly that the current achieves the 63% of his maximal value, 3 A, in a time inferior to 5 ms.

3.2.3 Software

To control the electronic circuit previously explained, we decided on a simple approach, which later showed not to be perfect, but suitable for prototype testing. The choice made was to program in G, the language used by National Instruments[1] in their product LabVIEW. Adding to the LabVIEW software we also used the multifunction DAQ NI USB-6008 (see figure 3.9, white box on the left), more precisely four of its digital outputs. Varying between $5 - 0$ V the digital signals permit us to control the gates of the MOSFETs of the electronic circuit, allowing us to control the direction in which the current flows through the coils. Allied to this we used a special technique called Pulse Width Modulation, PWM (see figure 3.12), which allows us to reduce the average current flowing through the coils, using square waves with different periods, maintaining

---

[1]http://www.ni.com
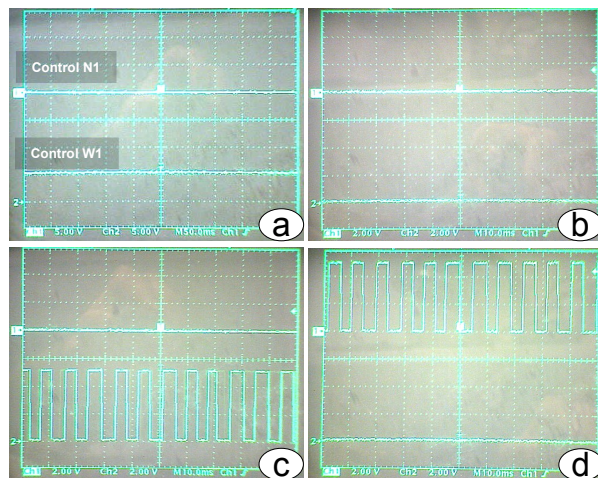
Figure 3.12: Pulse Width Modulation used to reduce average current in the coils and control the magnetic field's intensity. (a) Magnetic field directed at N with Control N1 at 0 V and Control W1 at 5 V, (b) Magnetic field directed at NW with Control N1 and W1 signals both at 0 V, (c) Magnetic field directed at NNW with Control N1 always at 0 V and Control W1 signal pulsing, (d) Magnetic field directed at WNW this time with Control W1 always at 0 V and Control N1 signal pulsing.

the MOSFETs in the saturation zone, which would otherwise be impossible seeing that the *on resistance* of the MOSFETs would be too big and the transistors would heat and malfunction. One problem with the NI 6008-USB device is its low output frequency capacity. Testing and measurement showed us that the device can only produce square waves up to 200Hz. This proved to be inferior than the needed because a small parasite vibration can be seen when moving the columns of beads.

3.3   Modes of Operation

All software was developed in the LabVIEW programming environment and coded in National Instrument's visual G language. Although this language presents some limitations in terms of efficiency, its visual approach simplifies the programming of a GUI (Graphic User Interface). As the electronic circuit only allows the manipulation of the direction of the current independently through each pair of coils, the following modes of operation were designed (see figure 3.13): *All Around*, *Alternated*, *Manual* and *Noise*.
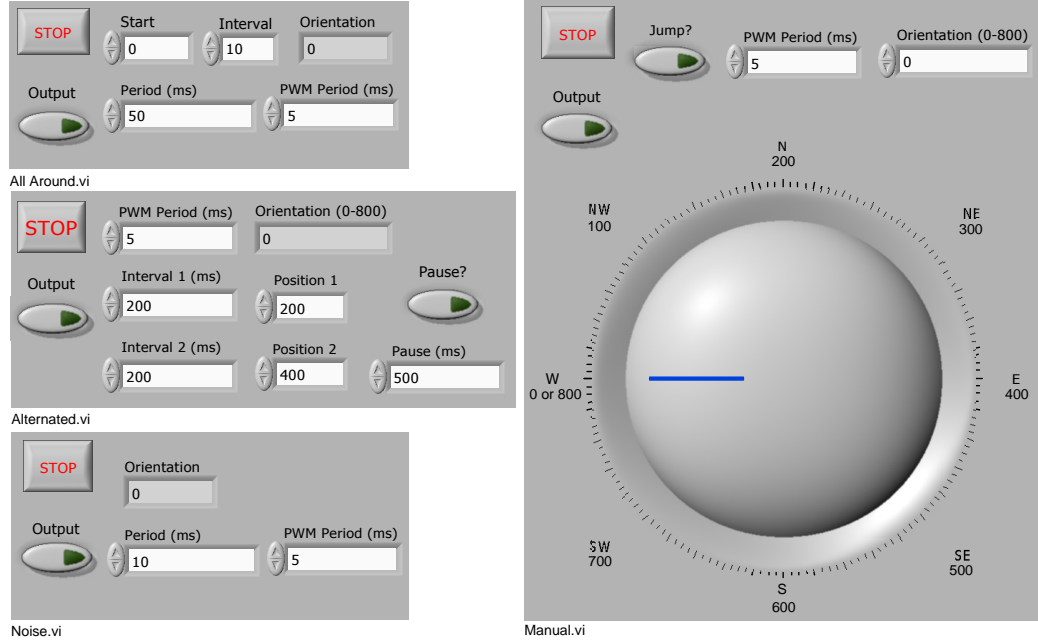
Figure 3.13: Partial view of the control panels of all operation modes. Complete and larger in Appendix B.

3.3.1 All Around

In the *All Around* operation mode, the idea is to automatically rotate the columns of beads, choosing the rotation frequency, direction of rotation and the interval of angular variation (see figure 4.6). The PWM technique is here used to permit the minimal angular rotation of 5°. This is achieved by turning one of the coils always on, and changing the period of the square wave that controls the passing of the current through the other. As an example (see left side of figure 3.15), when we want to have the magnetic fields' orientation between North and Northwest, we will have the vertical pair of coils always on, Control N1 at 0 *V*, and the other pair of coils, Control W1, intermittently on and off at a specific frequency (see figure 3.12.c). This signal is 5 *V* (the coil is off) at the N position (figure 3.12.a) and in the direction of NW the signal is pulsated at an increasing frequency. When the NW is reached, both coils are always on, meaning Control signals are both at 0 *V* (figure 3.12.b), with no pulsing occurring. Passing the NW position in the direction of W position, it's now the vertical coils' current which is pulsed (figure 3.12.d).

Figure 3.14: Two cases of the main module which is shared by all operation modes.
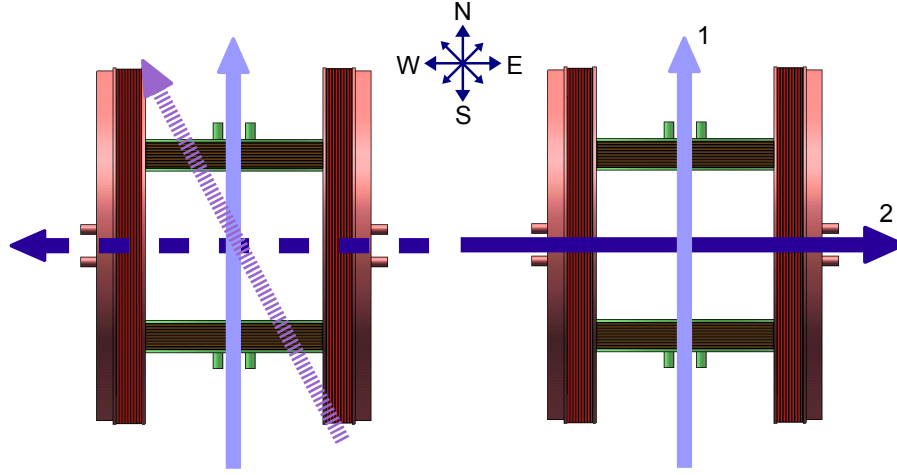
Figure 3.15: On the left side the visual explanation of the All Around operation mode. On the right the visual explanation of the Alternated mode.

At figure 3.13 we see its control panel. The control panel displays a few options. The **Start** option relates to the starting position of the rotation. The **Interval** option relates to the interval of angular variation the user wants. The **Orientation**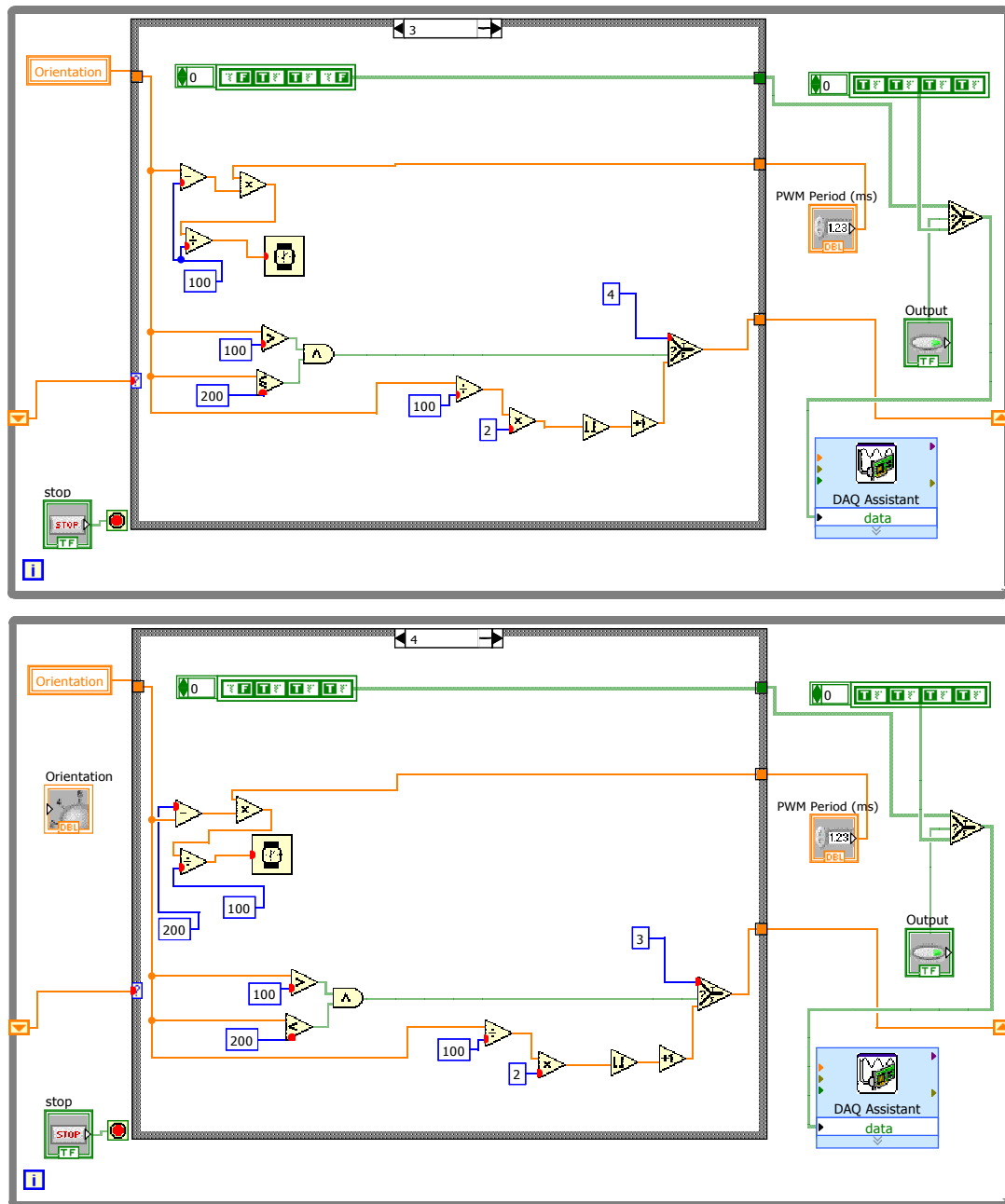 display shows us in which position and direction the magnetic field is oriented. It has values from 0 to 800, being 0 - West, 200 - North, 400 - East, 600 - South and 800 once again West. To better understand the relation between this numbers and the orientation please refer to the knob in Manual Mode control panel of figure 3.13. The **Period** option allows us to define the frequency of rotation, and finally the **PWM Period** option allows us to control the frequency at which the PWM is made.

As for code (figure 3.14), the All Around mode shares the main loop with all other modes. The loop represented by the gray rectangle is the module that controls the four NI USB-6008's output values by way of a boolean array, represented in green with the letters F and T representing False and True, or 0 V and 5 V. As previously said, the False, or 0 V, position means that the specific current controlling MOSFETs are conducting. So we have that the first output controls the current that flows through the coils in order to produce a magnetic field oriented to North. The second output orients the magnetic field to South. The third output orients the magnetic field to East and finally the fourth output orients the magnetic field to West. It consists most importantly of a 16 cases case. Each case controls 1/16 of the 360° angular area where

the magnetic field can be oriented. On this specific figure, 3.14, we have only two of these cases, number 3 and number 4. Using once again the previous example, where we want to have the magnetic field oriented between North and Northwest (figure 3.15, left side), we can now see what happens at the code level. In both cases we have the first letter of the array as an F, this means the vertical coils are making a magnetic field oriented to North. What happens now is that depending on the PWM period (showed right on figure 3.14) and orientation desired by the user (left on figure 3.14), we will have the timer, represented by a wristwatch inside a yellow square, a portion of the time on one case and another portion on the other. The more we want the orientation to approach North the less time the program will spend on the case number 3, and the more time on the case number 4. Both these times will always add to the time selected as the PWM period. The same explanation applies to all directions and to all different operation modes, changing only the way the orientation is controlled.

3.3.2 Alternated Mode

The Alternated Mode (figure 3.13 and 3.15, right side), is the mode that comprehends the original intension of this work: the separation of the particles. From its control panel we can see that two different orientations can be chosen for the magnetic field, **Position 1** and **Position 2**, and that the time in which the magnetic fields stay in that position is independently controlled, **Interval 1** and **Interval 2**. Adding to that there is the possibility of making a **Pause**, turning the magnetic field off, after the change of position, meaning: **Position 1**, **Position 2**, **Pause**. For the separation of the particles one uses normally positions which are 90° apart from each other. When we want to vibrate a column of particles, it is then wiser to choose two positions not very spread apart. The introduction of the **Pause** option has to do with the study of the influence of the Brownian motion on the particles behavior. Allowing a time, without any magnetic field, between position change helps us understand the influence of this thermal vibration on the particles and it was this influence that permitted us to discover the non-superparamagnetism of the Epoxy beads.

This modes also permits the vibration of columns of beads. If Position 1 and Position 2 are set to be close, the columns of beads will vibrate with the frequency defined by the interval times 1 and 2.

3.3.3 Manual Mode

The Manual Mode (figure 3.13), provides as the name says, manual operation and selection of the orientation of the magnetic field by means of the manipulation of the knob showed in the picture. By allowing the user to rotate the columns of beads freely it can be used to agglomerate various beads to form columns or various columns to form sheets, allowing the possibility of constructing simple structures using the beads available in the surroundings.

3.3.4 Noise

The last operation mode, is called Noise, figure 3.13. What it does is randomly select an orientation for the magnetic field, at a chosen frequency.

3.4 Conclusion

In this chapter we explained the design, construction and functionality of the system. Its structure and specifications were presented as well as its limitations. The temperature dependence of the magnetic field generated by the Helmholtz coils and the consequent need for a cooling system was discussed and the decisions made explained. This system was described and it was accepted that it is not enough to completely cool the system. Although not sufficient to completely cool the system, this compromise was accepted to agree with the other specifications. The magnetic field's intensity and uniformity was simulated and calculated and found acceptable in the working area. The control system was also explained in this section. The end result was a simple yet powerful computer controlled electronic circuit. The implementation of the PWM technique improved the system's capability and permitted us to develop complex operation modes. These operation modes were programmed using NI LabVIEW's graphic language G and permit the control of the superparamagnetic microparticles in various ways as described: rotation, separation, vibration and agglomeration.

4

Experiments and results

4.1 Sample Preparation

The setup for the experiments was a microscope with two possible objectives: 20x and 100x (oil immersion lens). The sample preparation was made in two different ways. Shown in figure 4.1 are representations and actual pictures of the setups. On the left the mixture of water, particles and cells is enclosed between two 25 mm diameter glass plates which are in turn separated by a crown disc of silicon with a center area with 15 mm diameter and a height that can be 0.5, 1.0 or 2.0 mm. The volume of the sample is 85 μl for the 0.5 mm height crown disc. On the right side, the two glass plates are separated by a 'square' of grease. The volume of the sample varies but is in the order of 40 μl. Both sample methods have an opening, in the ring or grease to allow the mixture to be at atmospheric pressure.

With the help of a moving table the sample is moved over the objective and the visualized area is always maintained at the center of the magnetic field, where it is most uniform.

4.2 Operation Modes

To test the system, we began by testing its operation modes with different types of beads. The mixtures used varied in concentration and types of beads and in the output frequencies, not only of the rotation or change of the field but also of the PWM frequency.

After some experiments we conclude that the best results are obtained when the PWM
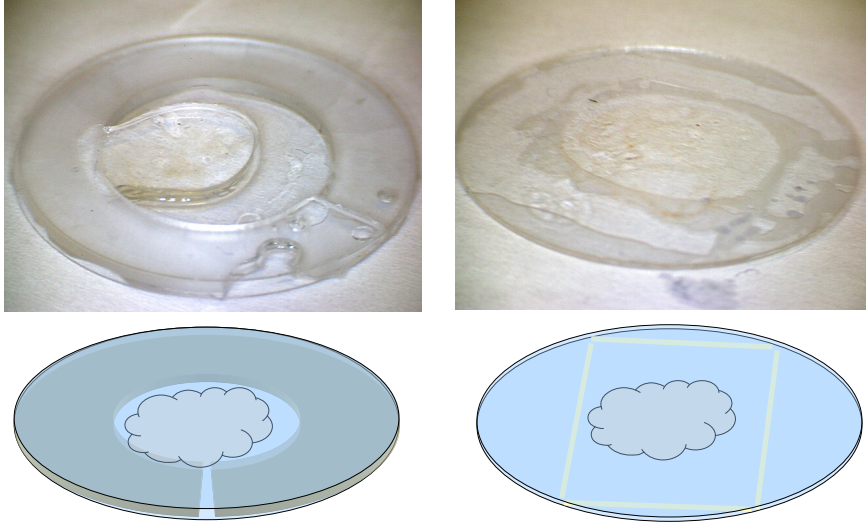
Figure 4.1: Sample methods used on the system.

frequency was the maximal allowed by the NI USB-6008 device for a square-wave which is 200 Hz. We use this value in the rest of the tests. It was visible that at lower values of PWM frequency, the parasite vibration of the columns would be bigger when the column was to be fixed at a certain direction. To have an idea of this parasite vibration we can glance at figures 4.2.5, 4.2.8 or 4.2.10.

4.2.1 Manual Mode

The most tested mode was the Manual mode (for the control panel refer to figure 3.13). It allows the manual control of the direction of the field. It can be used to rotate columns and sheets of beads or to separate them when the direction of the magnetic field changes by an angle between $45 - 90°$.

At figure 4.2 we have 2.8 μm Dynabeads, disposed in columns. Starting at 4.2.1 we see a column which is formed even though the field is zero due to a previously applied magnetic field and the small influence that the Brownian motion has on the 2.8 μm Dynabeads.

Figures 4.2.2 to 4.2.10 show us the rotation of the column following the direction change of the field. It is also clearly visible and due to the low capture frequency of the video camera, the parasite vibration of the columns when the field is not on one of the main

Figure 4.2: Manual mode with 2.8 μm Dynabead particles at 100x. At picture 12 an unwanted variation on the direction of the field induces a bigger jump than desired and consequently breaks the column.
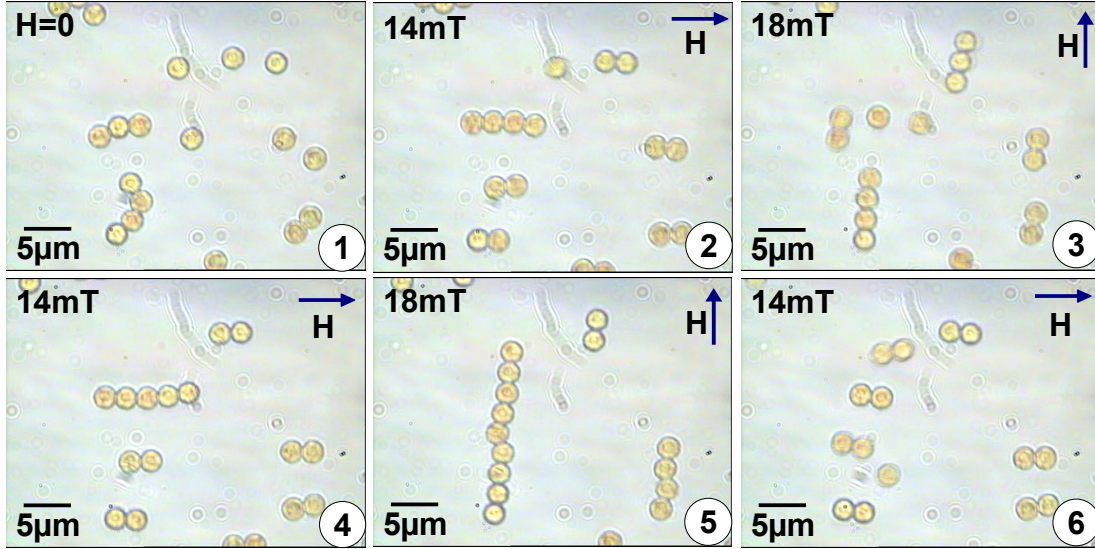
Figure 4.3: Alternated mode with 2.8 μm Dynabead particles at 100x. The sequential images show the separation of the particles when the direction of the magnetic field alternates between North and East (90°).

axes, namely: N, NE, E, SE, S, SW, W or NW. This happens because of the low frequency output capability of the NI USB-6008 device, which is in the order of the relaxation time of the coils. At the main axes we have no parasite vibration because no PWM is used as previously explained.

An interesting phenomenon happens at figures 4.2.10 and 4.2.11. The column increases its size after a small column, composed of 3 beads is attracted to the end of the bigger column. The manual mode permits us to build columns of variable size.

At figure 4.2.12 we see a breaking of the column. A slip of the hand while controlling the software made the field change its direction more than desired which resulted in the variation of the internal magnetic dipoles of the beads, resulting in their spreading. The output frequency stability of the NI USB-6008 is in fact also poor, and can also cause such problems. If the frequency of the PWM is temporarily decreased, the parasite vibration increases and the columns eventually break as happens again at figure 4.2.21.

4.2.2 Alternated Mode

This mode of operation was the first to be thought and planned and the first to be programmed. Even though the first attempts differ from this last version, the idea
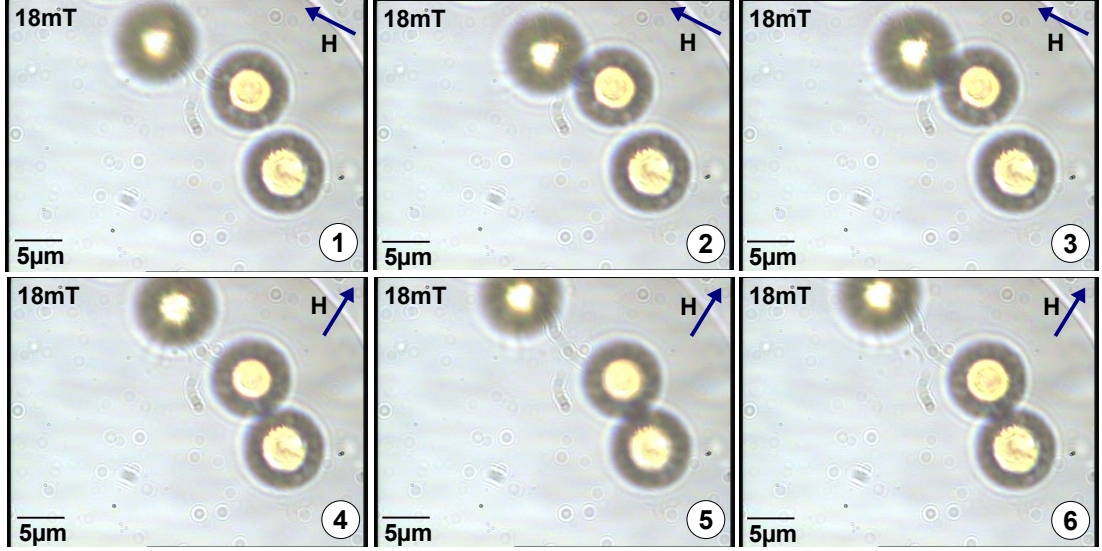
Figure 4.4: Alternated mode with 11 μm MicroParticles beads at 100x.

behind the mode is still the same. Alternate the direction of the magnetic field in order to separate the beads.

The mode is very versatile in the way that it permits the alternation of the fields between two directions freely chosen. In figure 4.3 we see this mode in action with the settings indicated in figure 3.13. The field's direction changes from N to E and it stays at each position for 200 ms. The figure 4.3 shows only the six first changes of the field, this is however a continuous operation. On this experiment the Pause option was not activated. As we see in the figures taken, with a 100x oil objective, the separation is not perfect, the particles do separate when the fields are changed, but they separate in groups. Normally in groups of 2 to 3 particles. As can be seen on the top of figures 4.3.5 and 4.3.6 a group of two particles will simple rotate according to the magnetic field. This is due to the relaxation of the current that flows through the coils which permits the bead pair to rotate following the change of direction of the magnetic field. Another experiment with alternating fields is shown with the 11 μm beads in figure 4.4. This time the sequential images show the separation of the particles when the direction of the magnetic field jumps 90° between NW and NE.

This mode also allows the vibration of columns. An example of this possibility is shown in figure 4.5. The Positions are this time N and NW and their intervals are 50 ms. The
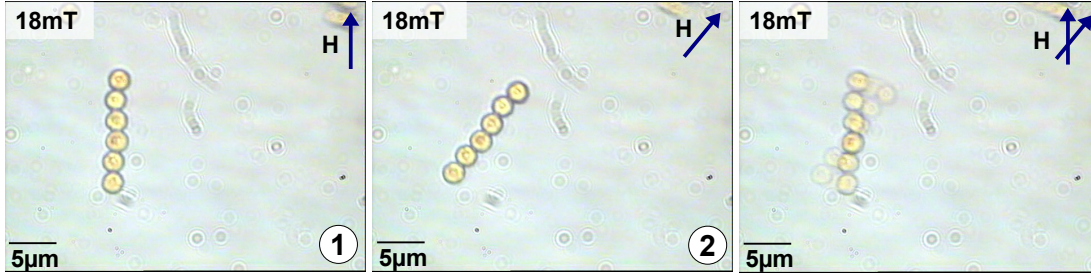
Figure 4.5: Alternated mode vibration of 2.8 μm Dynabead particle columns at 100x.

two first sequential images show the vibration of a column of beads. The direction of the magnetic field is changed $40 - 45°$. The picture on the right shows us an artifact generated by the caption frequency of the video camera, without any physical meaning it is shown because it is useful to have the notion of movement.

4.2.3 All Around Mode

The All Around mode offers the same control of the Manual Mode, but with the possibility of increased rotation speed and automated rotation. It also offers the possibility of Alternated control, when the Interval (see figure 3.13 for its control panel) is set to 200, the equivalent of $90°$). In figure 4.6 we have Epoxy beads being rotated using this operation mode with the settings as shown in figure 3.13. Of note is the bending and twisting of the columns due to non-superparamagnetic behavior. This twisting and bending originated what we called the agglomeration of beads and the formation of sheets of beads as is explained next.

4.3   Columns and Sheets of Beads

One particularity encountered on the behavior of the beads was the formation of columns and sheets when these interact with each other. This behavior occurred in all operation modes and with all types of beads, being the Epoxy beads the ones that showed more propensity. On figure 4.7 we can see two sequences where both phenomena occur. On the upper sequence we start with the 1.0 μm MyOne Dynabeads with no magnetic field applied. The figure 4.7.a2 shows what happens when the field is applied with the direction North. The beads approximate one another and start forming
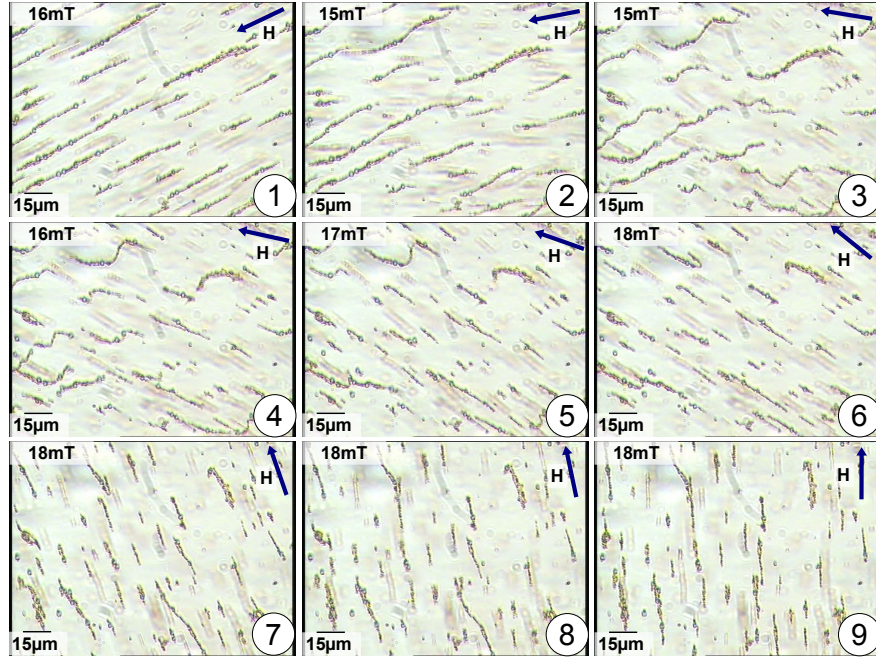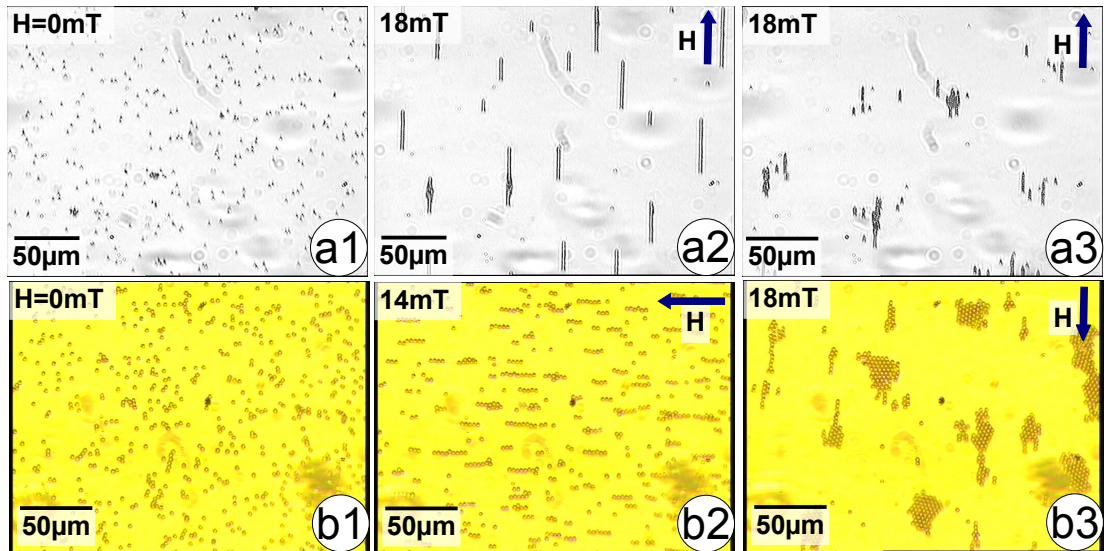
Figure 4.6: All Around mode on the Epoxy Beads.

Figure 4.7: Formation of columns and sheets.

columns. This is due to the appearance of the stray field previously explained. In this specific sequence **a**, the operation mode used was the Alternated. In figure 4.7.a3 is shown what happens after some minutes of operation. The bead columns will attract each other and begin to form sheets.

A similar behavior can be seen on figure 4.7 **b** sequence. This time the operation mode used was Noise and 2.8 μm Dynabeads controlled. Starting again with a zero intensity field, figure 4.7.b1, the beads form linear columns in the direction of the field applied, figure 4.7.b2, and after some minutes sheets start to form in figure 4.7.b3.

This behavior difficults the operation of the system when the intention is the separation of the beads. It nevertheless helps us when we want to move or rotate cells.

4.4 Moving Cells

The process of moving cells was found to be a arduous and very difficult task. Either the cells would stick to the glass surface or they would be too big to be moved. Nevertheless some movement was observed which shows the potential of the system (sequences in figures 4.8, 4.10 and 4.11). The following sections show a very qualitative collection of experiments.

4.4.1 Fibroblast Cells

The Fibroblast are connective tissue cells that synthesize a type of extracellular matrix rich in collagen and other macromolecules. They play an important role in animal wound healing. Its life span, measured in chick embryos, is 57 ± 3 days [24].

Being available at our laboratory, and a kind offer from our colleagues, we prepared a mixture of the fibroblast cells and the Epoxy beads. Figure 4.8 shows a sequence of pictures taken in one of the experiments, in this case using the All Around operation mode. Some of the beads connected to one of these cells and it was possible to move it. The precision of the movement was poor as can be seen in the sequence. The cell did not move smoothly with the changing magnetic field. It did nonetheless move in counter-clockwise direction, following the magnetic field.
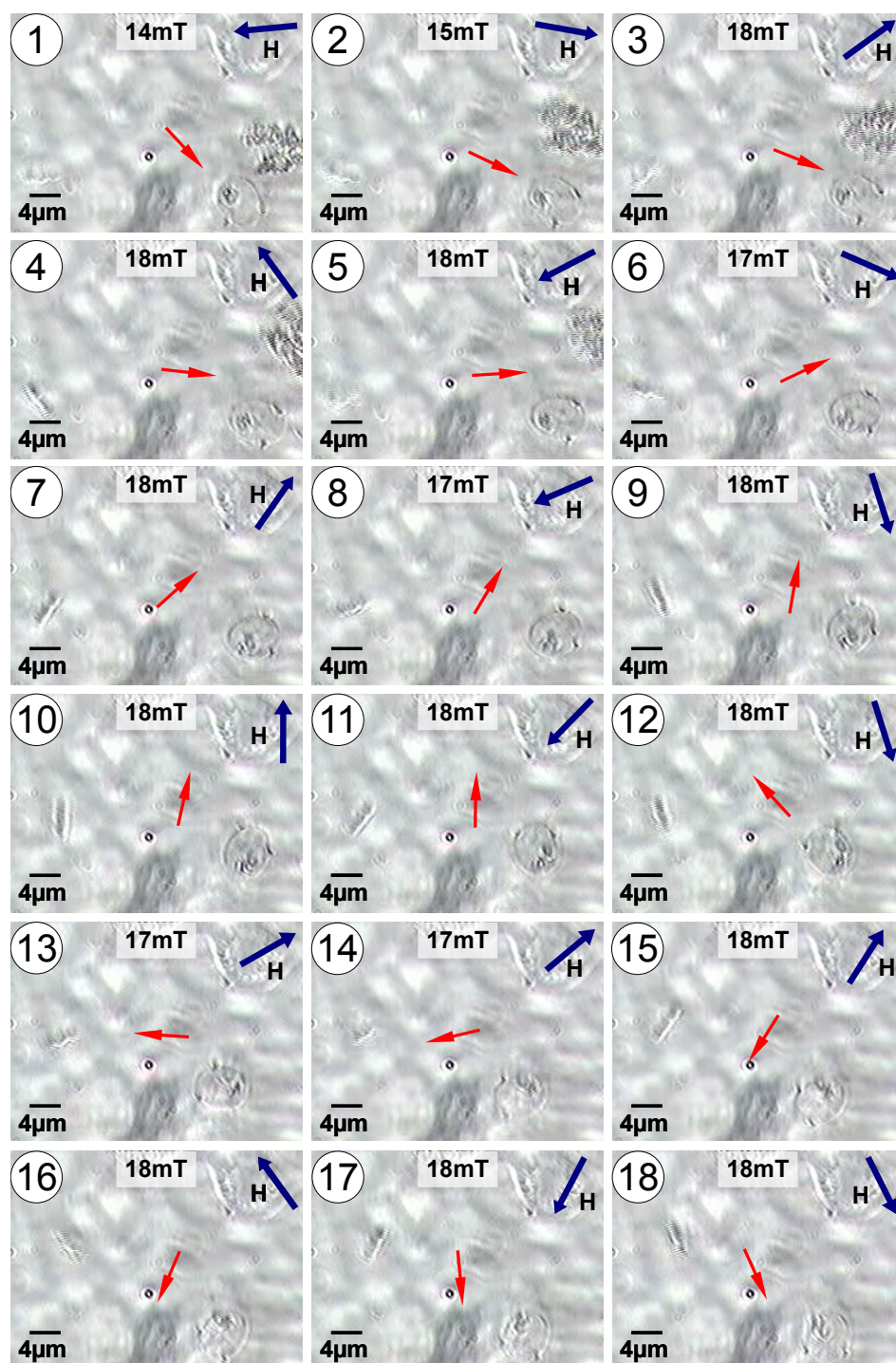
Figure 4.8: In a preparation of fibroblast cells and Epoxy beads at 20x and using the All Around mode, we could see a counter-clockwise rotation movement of a fibroblast cell. The red arrow indicates the cell at picture one and its rotation on the following pictures.
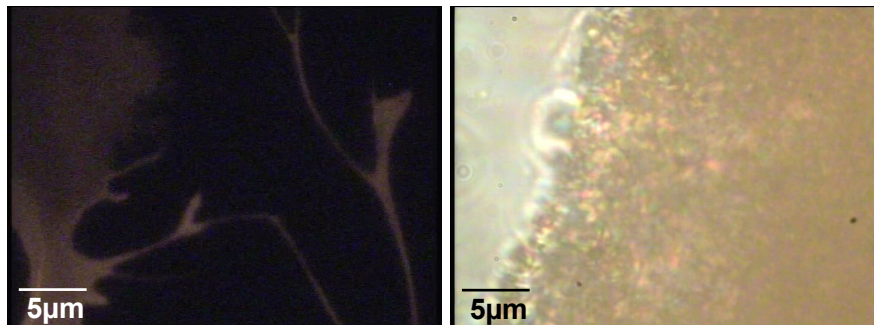
Figure 4.9: Sample with a mixture of Actin filaments and Epoxy beads. On the left the fluorescence image of the filaments. On the right the agglomeration of the Epoxy beads because of the high density solution.

4.4.2 Actin Filaments

A failed attempt but, worth describing, was the attempt to move Actin filaments with the help of the Epoxy beads. In collaboration with a PhD student colleague of our department, studying the formation and connections between Actin filaments, the following experiment was tried. Mixing Epoxy beads and a solution of Actin filaments, we tried to move the crossing filaments in order to discover if the superposed filaments are connected to each other (see left part of figure 4.9). What happened can be seen in the right picture of figure 4.9. The solution being too dense, impeded the movement of the beads.

4.4.3 Plant cells

At an attempt to test the system with all available cells and organisms, a mixture was made using once again the Epoxy beads and a drop of water provenient from a nearby lake. The water from this lake, being filled with bacteria, and other micro organisms was the perfect medium to experiment with the different modes.

From all the experiments made, the most interesting, and one of the few actually recorded, is the one showed in figure 4.10. Using the All Around operation mode, and having the Epoxy beads rotating in a counter-clockwise direction, the movement of a plant cell was detected and controlled. This time not due to the connection of the beads to the cell, but to the help of sedimented bigger Epoxy beads that served as a base on which the epoxy beads columns would rotate and further push the plant cell.
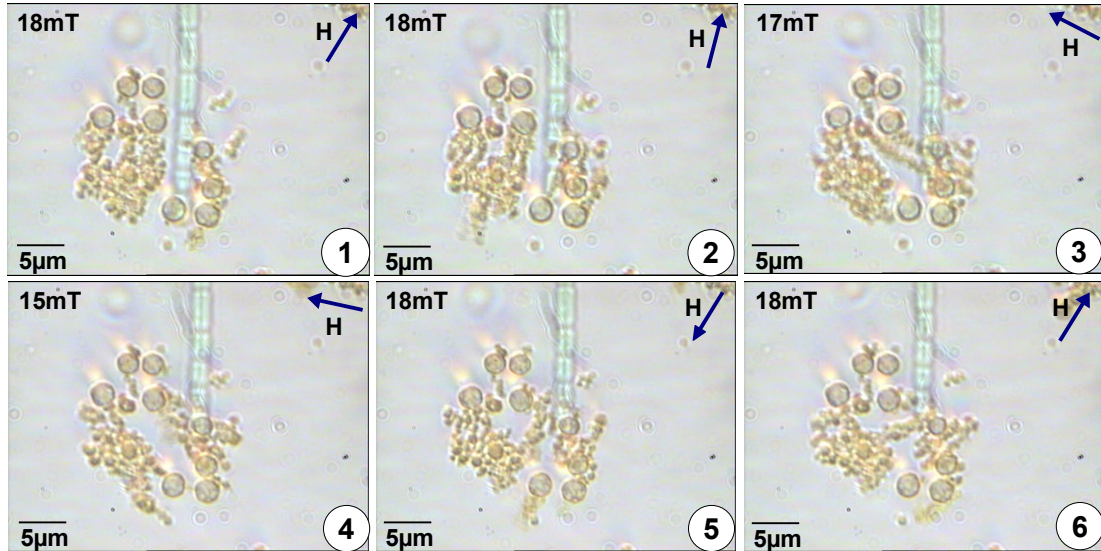
Figure 4.10: The Epoxy beads rotated counter-clockwise in the All Around mode permit the movement of what seem to be plant cells (100x). The mixture is composed by Epoxy beads and water taken from the Cospudener See, a lake nearby Leipzig.

4.4.4 Artemia

In order to test the range of sizes in which the system can operate, experiments with 200 to 300 μm long Artemia larvae were made. The concentration of the Epoxy Beads in the mixture was this time increased greatly. The All Around mode was used to rotate them at high frequency (with the settings, Interval: 30 (of 800), Period: 25 ms and PWM period: 5 ms). The results are in figure 4.11. The Artemia, being a living moving organism, would move in straight direction when the magnetic field was off and would rotate when the magnetic field was on. This can be explained, to our understanding, by the formation of sheets of beads were the larvae would lay. Rotating these sheets would then impede the larvae of effectively propulsion itself. This, having no direct utility was nevertheless useful to test the limits of the system in terms of order of magnitude and it showed us that the formation of sheets is useful in situations were the magnetic forces of just a couple of beads would not suffice.
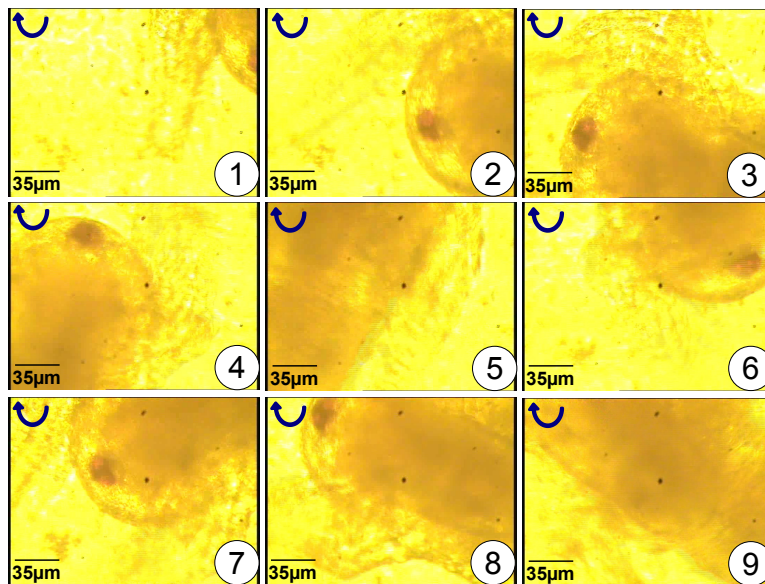
Figure 4.11: Mixture of living organisms called Artemia with Epoxy beads. The movement of the organism is influenced by the All Around clockwise rotation of the beads.

4.5 Conclusion

In this section we partially demonstrated the system's capabilities. The first section focused on the movement and control of the superparamagnetic microparticles and the problems that derive from their behavior with the formation of columns and sheets. In the last section we showed part of the experiments made with the particles and different types of biological objects. With this experiments we intend to show the system's versatility. The biological objects varied in size and shape and the system showed itself robust and adaptable to these different paradigms.

5

Conclusions and Future Work

5.1 Conclusion

In this work a novel system of magnetic tweezers was designed, constructed and tested. It is composed by two pairs of water cooled Helmholtz coils for the magnetic field generation, the electronics and software that control them, the precision table used to move the samples, the sample holder and by a fluorescence inverted microscope where the Helmholtz coils, the precision table and the sample holder are mounted. This apparatus had to fulfill the size restrictions of the fluorescence microscope on which it was mounted. The magnetic field's intensity and orientation can be controlled in all directions inside a plane composed by the central axes of the four coils. This magnetic field controls superparamagnetic microparticles that control biological objects.

In the second chapter, we explained the physical concepts necessary for understanding the system's functionality and the behavior of the microparticles in these fields. The characteristics of the magnetic field generated were studied and calculated as well as the forces derived from the gradients formed by the presence of these superparamagnetic microparticles. The microparticles were also studied and their different types and characteristics measured and explained.

The third chapter is focused on the description and operation mode of the system. The different constituents were shown and explained, the two Helmholtz coils, its water cooling system, the microscope's supporting table, the moving table and sample

holder, the lighting system and the video camera all mounted in an inverted optical microscope. The electronic controlling circuit with its computerized control made with the help of the National Instruments' USB-6008 DAQ are also present. The system permits more than one operation mode. For that a dedicated software was developed in LabVIEW.

The fourth chapter is dedicated to show the capabilities and function of the system. First, the different operation modes of the system and how they can be used to control the microparticles are shown and the particles' behavior explained. Some qualitative experiments involving biological objects such as fibroblast cells, plant cells, actin filaments and finally a living artemia larvae organism, are shown.

In the present chapter we discuss what was learned and discovered about the characteristics of the superparamagnetic microparticles. We evaluate the system's performance and discuss it's capabilities and limitations and how it can be improved in the future.

The study of the characteristics of the superparamagnetic microparticles was the start to understand how to develop the system. The bibliography available was crucial to the understanding of their behavior in dynamic magnetic fields and the tests as well as the AFM and MFM techniques. The experiments made with the beads helped us to determine which type could be used for each purpose. The discovery of the non-superparamagnetic behavior of the Epoxy beads was very important in the way that it was then possible to understand behaviors that were until then difficult to explain.
The different sizes of the beads helped us understand the dependence of the system's performance on this characteristic. The increase in size, and therefore the increase in the quantity of magnetic material, increase the forces between the beads and increase the effect these have on the biological objects.
The difficulty in separating the beads that we encountered in developing the Alternated Mode opened our options and permitted us to develop the other operation modes. Initially intended to have only one separation mode, the system gained new capabilities and the possibilities of microparticle control greatly increased with the new modes.
In order to achieve the different operation modes, the control electronic circuit had to

be done and redone a number of times and the controlling software was also continuously improved with the final results shown in the work. The implementation of the PWM capability increased the rotation precision of the system and the possibility of controlling the magnetic field's intensity while maintaining the power MOSFETs operating at the saturation zone. This was necessary as previously explained due to the high current used.

The system has nonetheless its limitations and one of them is the output frequency limitation of the electronic device used, the NI USB-6008, that for a prototype testing was suitable, but lacks on high frequency (frequencies in the order of $\sim kHz$) output capability and on output stability. As explained previously, this limits the precision of the angular variation of the magnetic field, on the Manual and All Around modes, inducing parasite vibration of the columns of particles due to the relaxation times of the coils, which are between 1.0 and 1.5 ms (as in figure 3.11), which are smaller than the maximal frequency output capability of the NI USB-6008 device, which is of 200 Hz. This in terms of rotation means that while the magnetic field is pulsating, with PWM in use, the minimal period of the pulses will be more than two times bigger than the relaxation time of the coils, reducing the effectiveness of the PWM technique.

Still playing an important part on the system's limitation, the relaxation time due to the impedance of the coils is now too slow. In order to successfully separate the particles in the Alternated Mode (as seen in figure 4.3), which requires relaxation times in the order of the hundreds of microseconds, the disappearance of the magnetic field will have to happen faster. This can be solved by reducing the size of the coils and consequently the current needed and the characteristic inductance, but this will decrease the force between beads resulting from the stray magnetic field. The new system will have to find an equilibrium between these two limitations.

The force between particles could also be higher if the space limitations and sample area constraints were not so strict. The forces vary considerably with the distance and size of the beads but also with the parameters of the coils. As the experiments that required force measurements were not made, these were not tested as intended. The measurement of the magnetic force requires a video analysis software which is not developed at this time but is present in our wish list.

In terms of the cooling system, it can still be improved greatly. As it was not a main concern (we just wanted something that could cool enough as to prevent burned fingers

during operation and to maintain the coils' resistance fairly constant), it was left to a second plane that will be looked at again in a further stage of the project.

In terms of the experiments with biological objects, as stated previously, the experiments showed are intended as qualitative and are a showcase of the capabilities of control that the system offers. One of the most wanted experiments was in fact not performed. The use of the Alternated Mode in order to perform experiments with DNA strands and other microsized macromolecules. This was postponed due to the development of the system and will be initiated in a near future. In order to do this the mechanisms necessary for the connection between the beads and the macromolecules has to be studied and experiments with more types of beads need to be performed.

5.2 Future Work

The future work and future developments intended include the design and construction of a new system while improving and experimenting with the present one. Improvements to the present system include adding a third pair of coils to have control in the three spatial dimensions. This way we can rotate cells and have a view of them in all intended directions. And not only on one plane as in the example of the fibroblast cell in figure 4.8.
Implement a different control device that allows PWM frequencies up to tens of kHz. With this capability the parasite vibration of the rotation operation modes will be greatly reduced and the precision of rotation increased. This also implies the reprogramming of all software in a new language, namely C++. The device Arduino Uno[1] presents itself as an open-source electronics prototyping platform with PWM capability.

The design of the new system will focus on the minimization of the limitations and of the major problems of the present system while trying to maintain the strength of the generated magnetic fields. With this new design we pretend to redo the whole system on a new microscope specifically designed for it. With that, the space limitations and focusing system will not be so strict and may be adapted to our requirements. We pretend to spread apart the coils to have a system composed of identical coils. A

---

[1]http://arduino.cc

cube can then be constructed with a coil in each surface. This will permit the consolidation of the system and eliminate the need for having a supporting table. A negative side of this idea is the decrease of the field's intensity and uniformity, but as seen before (in figure 3.8), the work area is small enough to have a good uniformity.

In the new system we will try to reduce the power dissipated by the coils in order to have a simple water cooling system. By reducing the size of the system, this need will be mostly fulfilled. The decrease of the current will also be a possibility. New calculations and mechanical designs have to be made.

Reducing the current needed to achieve the desired magnetic field may be an alternative to the use of the PWM technique. In order to have variation of field without the use of PWM this current can be reduced and the MOSFETs used in the linear zone. The current will then be linearly controlled without the need of a pulsed control signal.

Parallel to this the implementation of video analysis in order to measure forces, cell and DNA strand deformation and velocities and displacements will be initiated. A video analysis software will be developed.

The connection of the beads to the macromolecules and DNA strands will be deeper studied and implemented.

Finally the experiments with macromolecules as DNA strands or with cells, early stage fish eggs and protein filaments and every biological system that is in the order of some micrometers, will continue.

5. CONCLUSIONS AND FUTURE WORK

Bibliography

[1] F Ritort, TOPICAL REVIEW: Single-molecule experiments in biological physics: methods and applications, J. Phys.: Condens. Matter 18 (2006) R531-R583, (2006). 2, 13

[2] Kipom Kim, Omar A. Saleh, A high-resolution magnetic tweezer for single-molecule measurements, Oxford University Press (2009). 13

[3] Richard Feynman, The Feynman Lectures on Physics 2, Addison-Wesley, (2nd ed.), (2005). 6

[4] John David Jackson, Classical Electrodynamics, Wiley, New York, (3rd ed.), (1999). 7

[5] Martin A. Gijs, Frédéric Lacharme and Ulrike Lehmann, Microfluidic Applications of Magnetic Particles for Biological Analysis and Catalysis, Chem. Rev. 2010, 110, 1518-1563, (2010). 8, 13, 18

[6] L. Néel, Théorie du traînage magnétique des ferromagnétiques en grains fins avec applications aux terres cuites, Ann. Géophys. 5, 99136, (1949). (English Translation) 8

[7] P C Fannin and S W Charles, On the calculation of the Néel relaxation time in uniaxial single-domain ferromagnetic particles, J. Phys. D: Appl. Phys. 27 (1994) 185-188, (1994). 8

[8] Dinesh Martien, AC Magnetic Measurements, Quantum Design, (2000). 8

[9] Johannes Eisenmenger and Ivan K. Schuller, Overcoming thermal fluctuations, Nature, (2003). 9

BIBLIOGRAPHY

[10] J. I. Gittleman, B. Abeles, and S. Bozowski, Superparamagnetism and relaxation effects in granular Ni-SiO2 and Ni-Al2O3 films, Phys. Rev. B 9, 38913897, (1974). 9

[11] Charles Kittel, Introduction to Solid State Physics, Wiley New York, (1996). 10

[12] Ralph Skomski et al, Effective Demagnetizing Factors of Complicated Particle Mixtures, IEEE Transactions on Magnetics, vol. 43, no. 6, June, (2007). 11, 18

[13] Jean-Paul Fortin, Florence Gazeau and Claire Wilhelm, Intracellular heating of living cells through Néel relaxation of magnetic nanoparticles, Eur Biophys J (2008) 37: 223-228, (2008). 11

[14] Michael Barr, Pulse Width Modulation, Embedded Systems Programming, September 2001, p103-104, (2001).

[15] Raymond Serway and John Jewett, Principles of physics: a calculus-based text, Volume 1, Brooks/Cole, Thomson Learning, 4th edition, (2006). 12, 18

[16] Robert Brown, A brief account of microscopical observations made in the months of June, July and August, 1827, on the particles contained in the pollen of plants; and on the general existence of active molecules in organic and inorganic bodies., Phil. Mag. 4, 161173, (1828). 14

[17] Edward P. Furlani, Permanent Magnet and Electromechanical Devices: Materials, Analysis, and Applications, Academic Press, (2001). 16

[18] S. Chandrasekhar, Stochastic problems in physics and astronomy, Reviews of Modern Physics vol. 15, pp. 189, (1943).

[19] Mojca Vilfan, et al, Self-assembled artificial cilia, PNAS February 2, 2010, Vol. 107, 1844-1847, (2009).

[20] Y R Chemla, et al, Ultrasensitive magnetic biosensor for homogeneous immunoassay, PNAS, December 19, 2000, vol. 97, no. 26, 14268-14272 (2000).

[21] T. R. Strick, V. Croquette, et al, The Elasticity of a Single Supercoiled DNA Molecule, Science, vol 271, (1996).

[22] Nikolai Stankiewicz et al, In vivo labeling and specific magnetic bead separation of RNA for biofilm characterization and stress-induced gene expression analysis in bacteria, Journal of Microbiological Methods 79, (2009). 13

[23] Anthony H. B. de Vries et al, Patterned Electroplating of Micrometer Scale Magnetic Structures on Glass Substrates, Journal of Microelectromechanical Systems, VOL. 13, NO. 3, (2004).

[24] Weissmanshomer, P.; Fry, M., Chick embryo fibroblasts senescence in vitro: Pattern of cell division and life span as a function of cell density, PMID Mechanisms of Ageing and Development 4 (2): 159., , (1975). 48

Appendix A

Technical drawings

All technical drawings in this appendix were made using the software Solidworks[1].

A.1 Coils

A.2 Microscope table

A.3 Sample holder

A.4 Silicon rings maker

A.5 Light system extension

---

[1]http://solidworks.com

A. TECHNICAL DRAWINGS
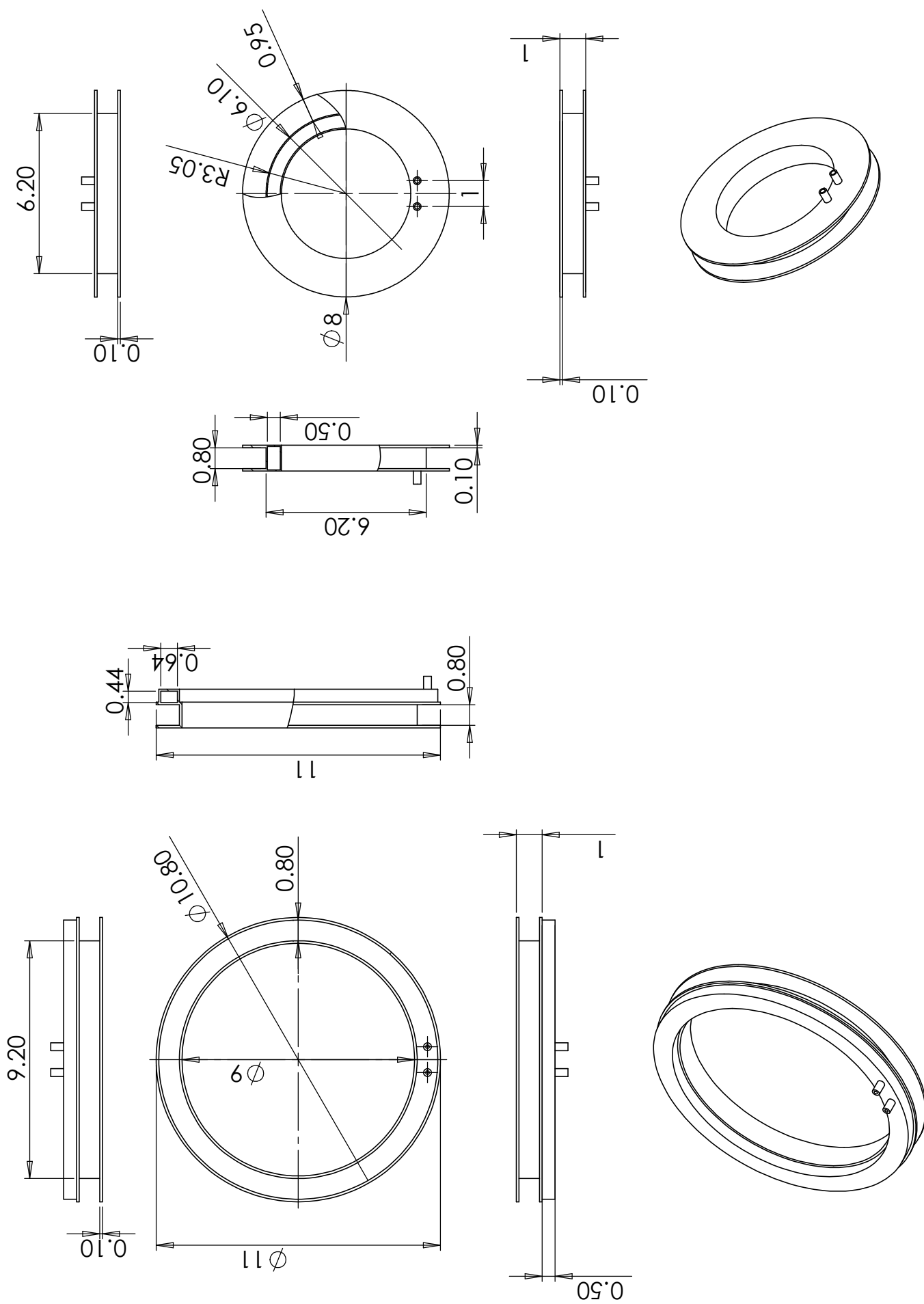
Figure A1.1 - Technical drawing of the Helmholtz coils.
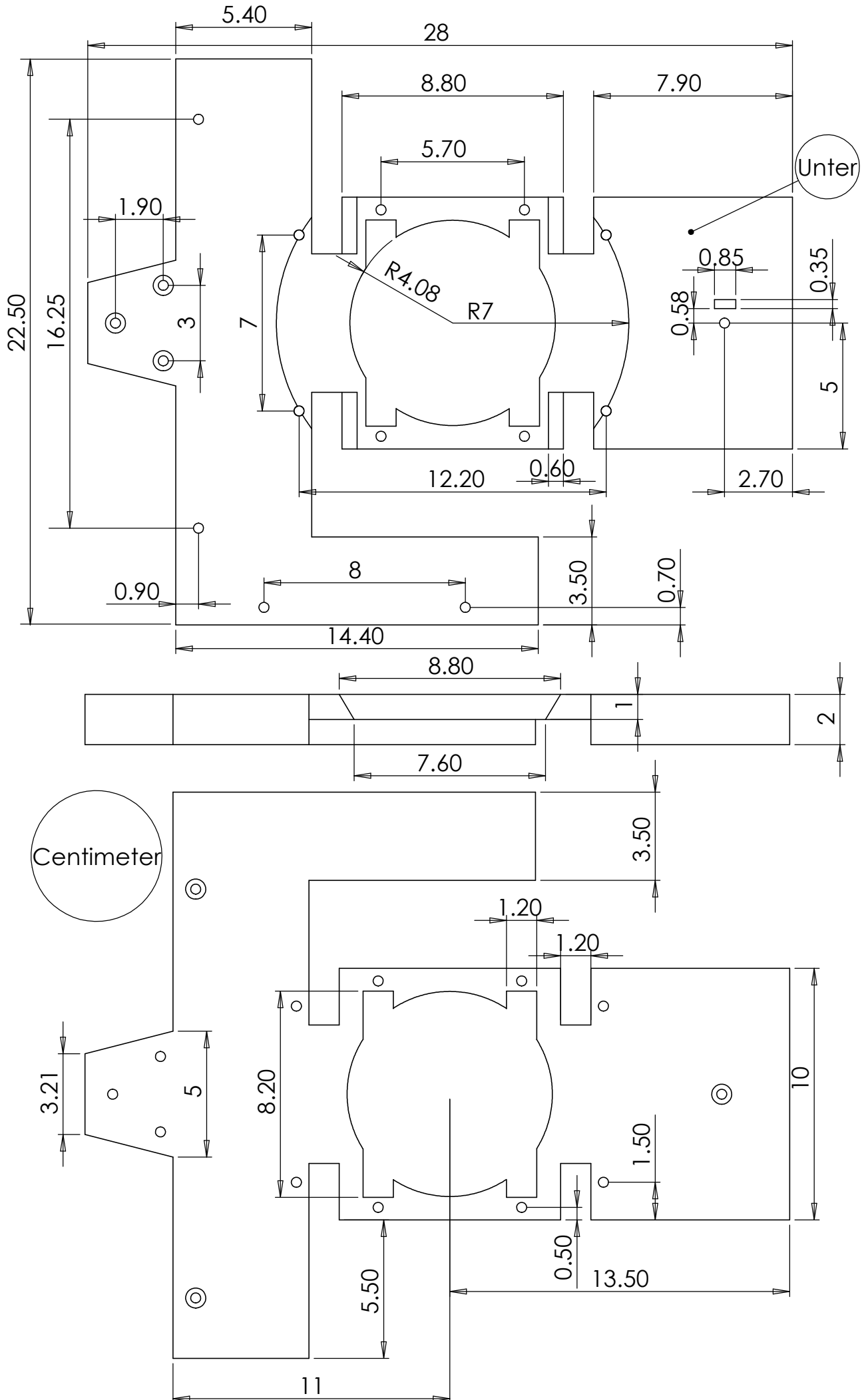
Figure A1.2 - Technical drawing of the supporting table.
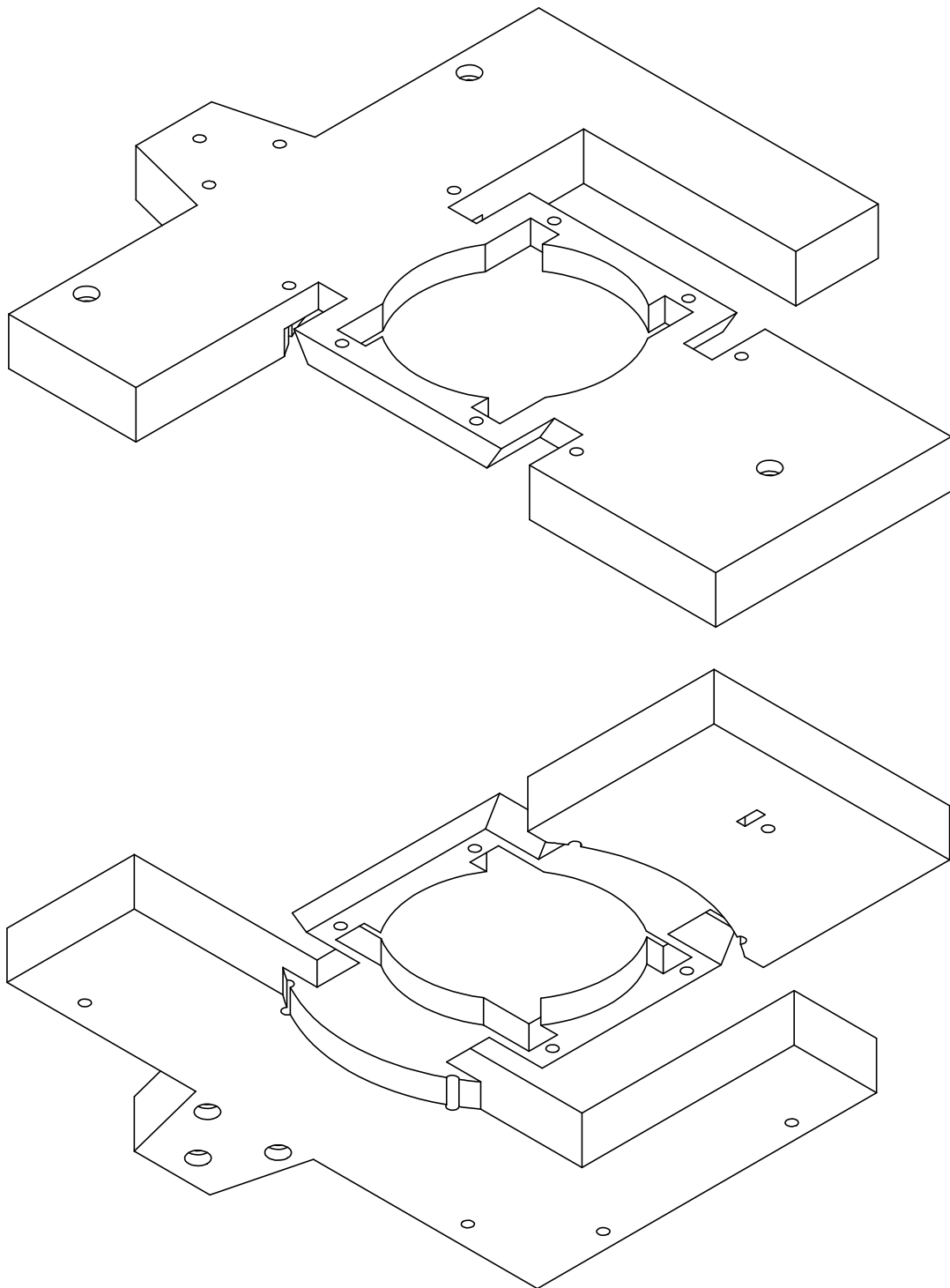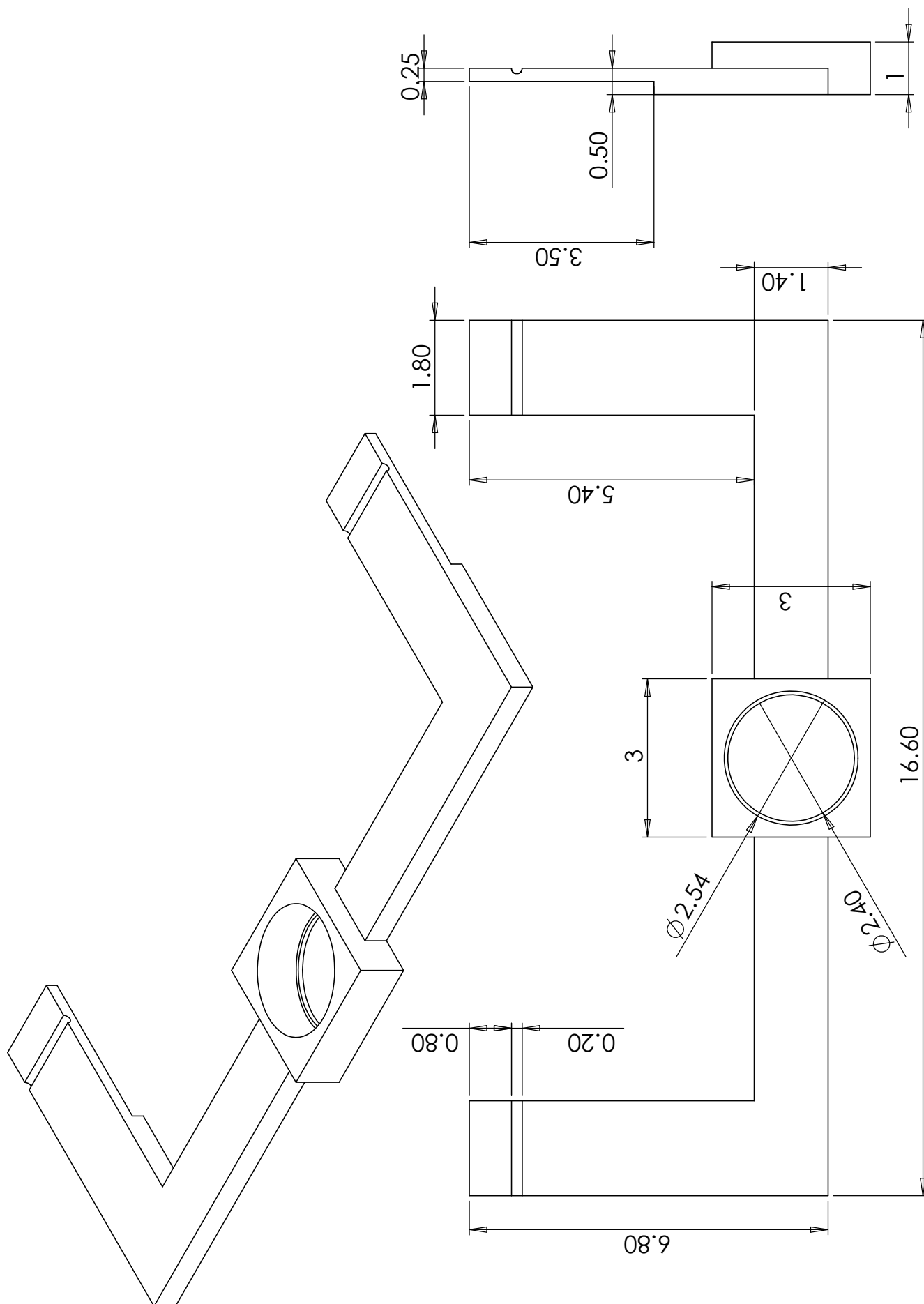
Figure A1.3 - 3D view of the supporting table.

Figure A1.4 - Technical drawing and 3D view of the sample holder.

R12.5

R7.5

Ø40

1.0

millimeter

0.5 / 1.0 / 2.0

5.0

5.0
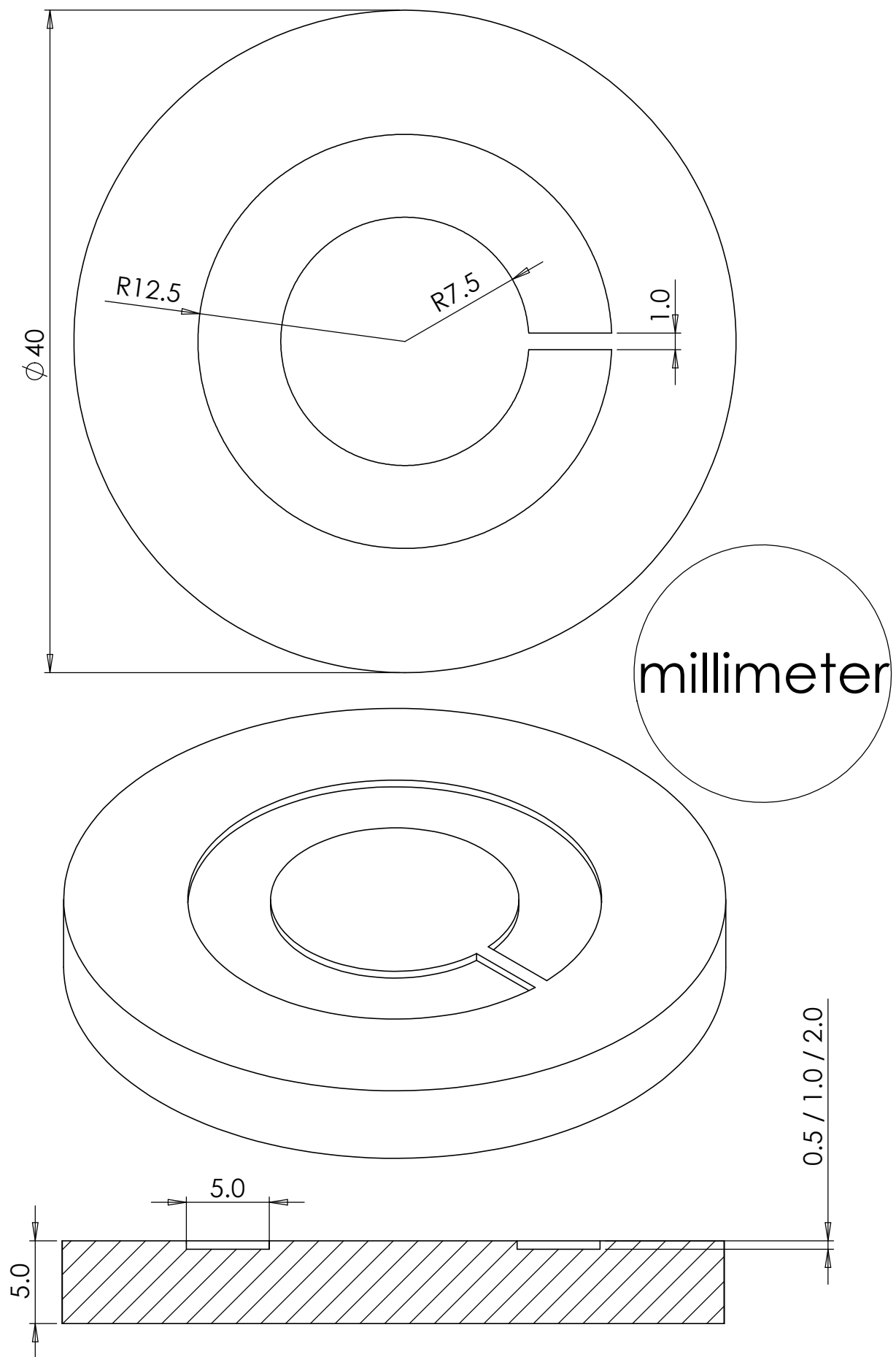
Figure A1.5 - Technical drawing and 3D view of the silicon ring form.

30

18

15

22

R10

20

15

20

30

50

15

50

30

30

millimiter
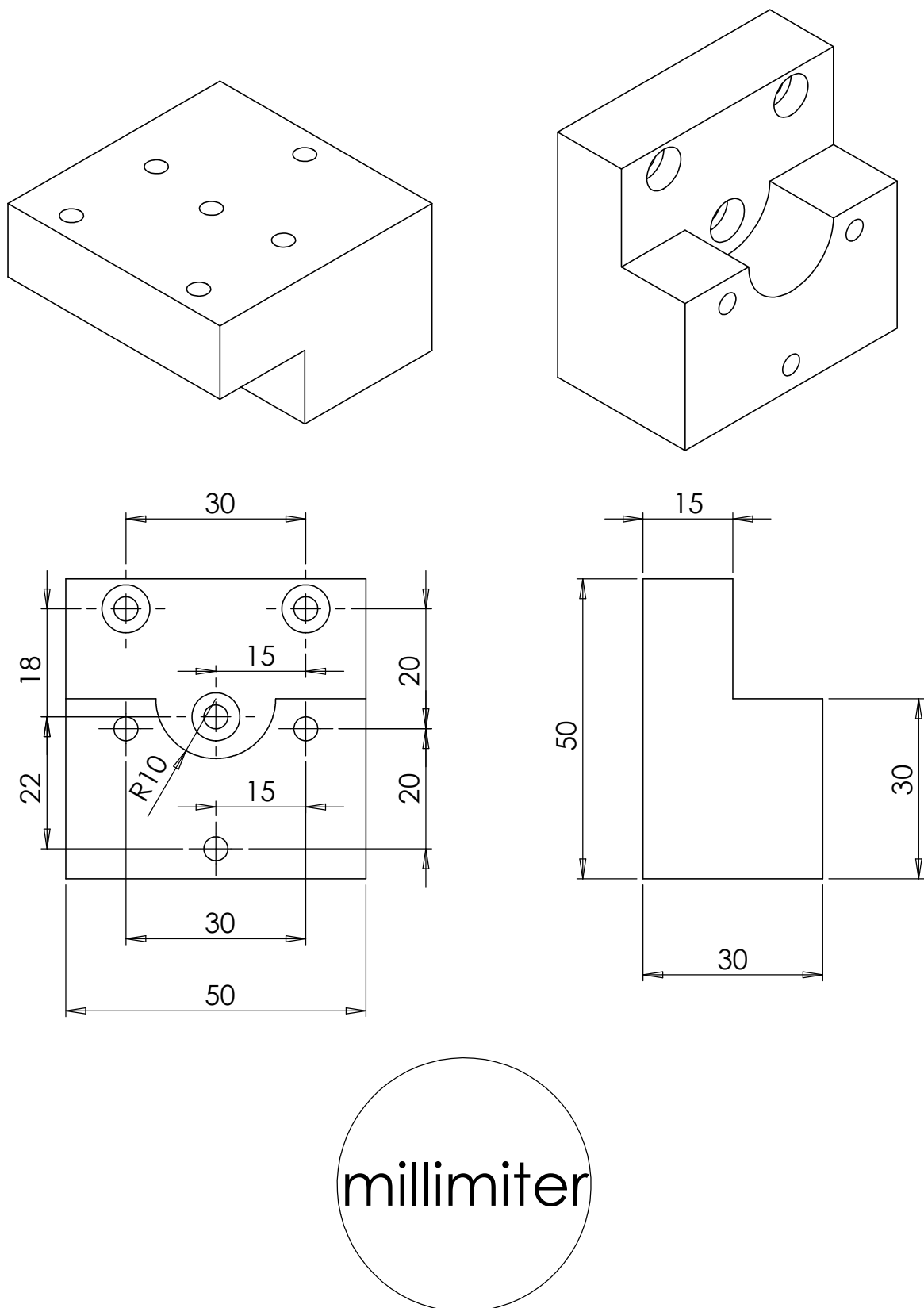
Figure A1.6 - Technical drawing and 3D view of the light extension.

Appendix B

Software and Source code

In this appendix is presented the source code for the control system programmed in G in National Instrument's LabVIEW[1].

B.1   LabVIEW

---

[1]http://ni.com/labview/

B. SOFTWARE AND SOURCE CODE

All Around.vi

STOP

Output

Start
0

Interval
0

Orientation
0

Period (ms)
10

PWM Period (ms)
5

No visuals | With visuals

N

NW   NE

0

W   E

SW   SE

S

N   S   E   W
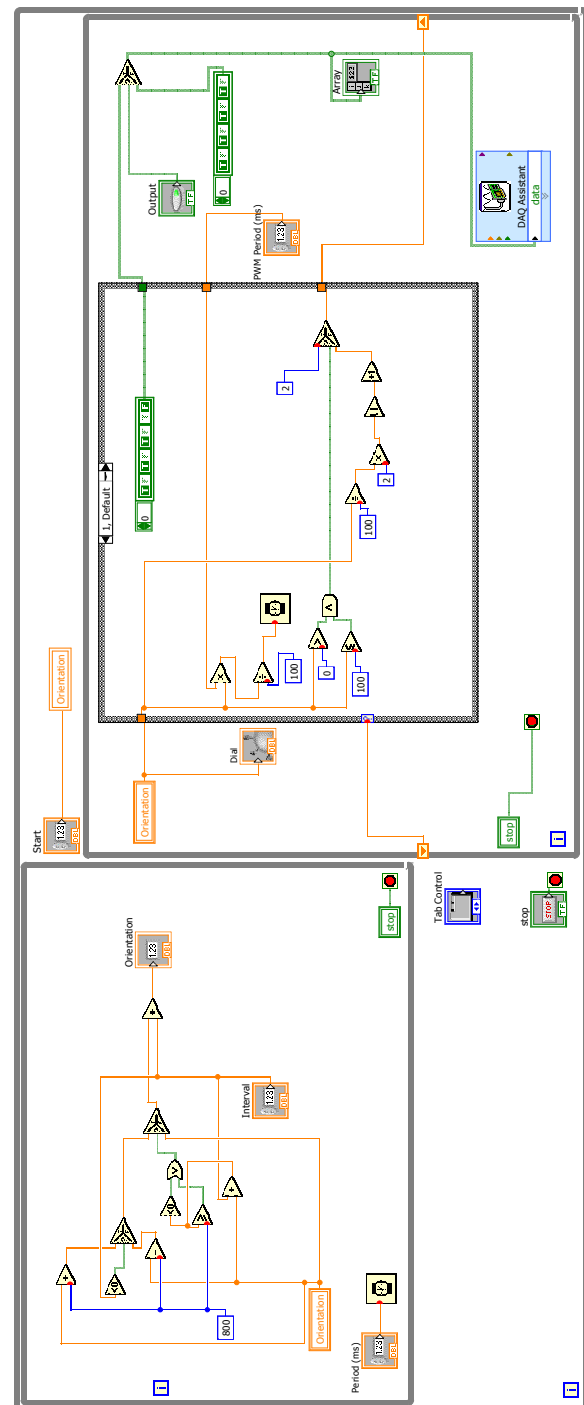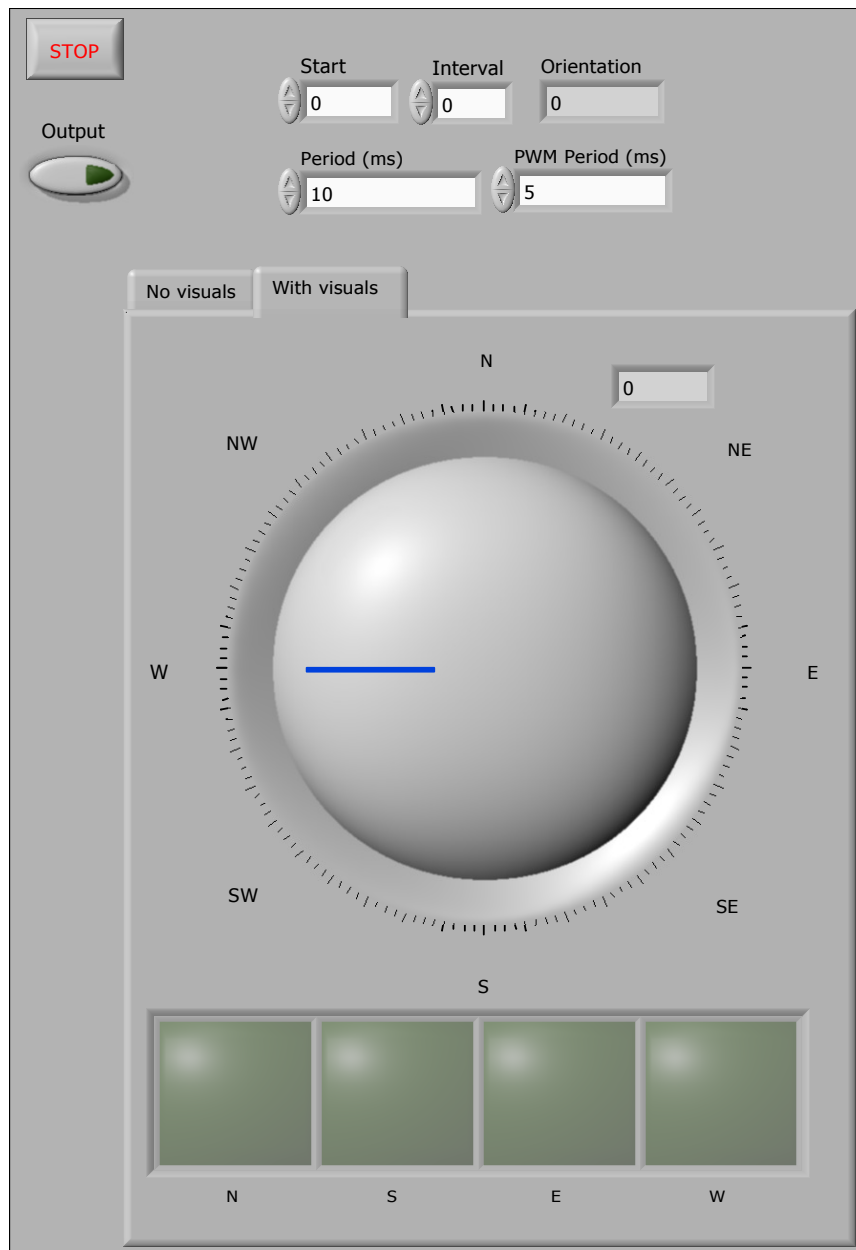
Figure B1.1 - All Around Mode: control panel and source code.
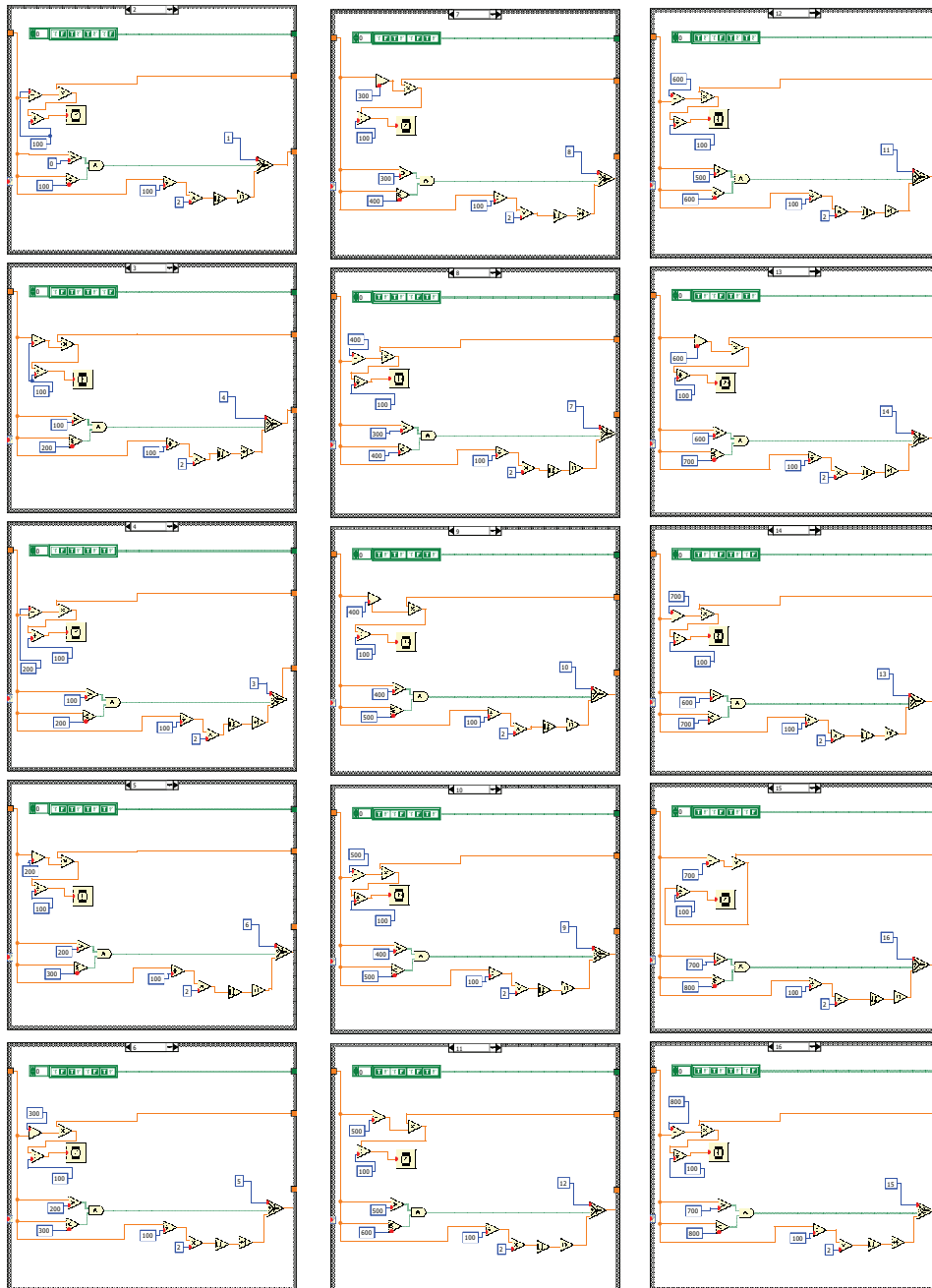
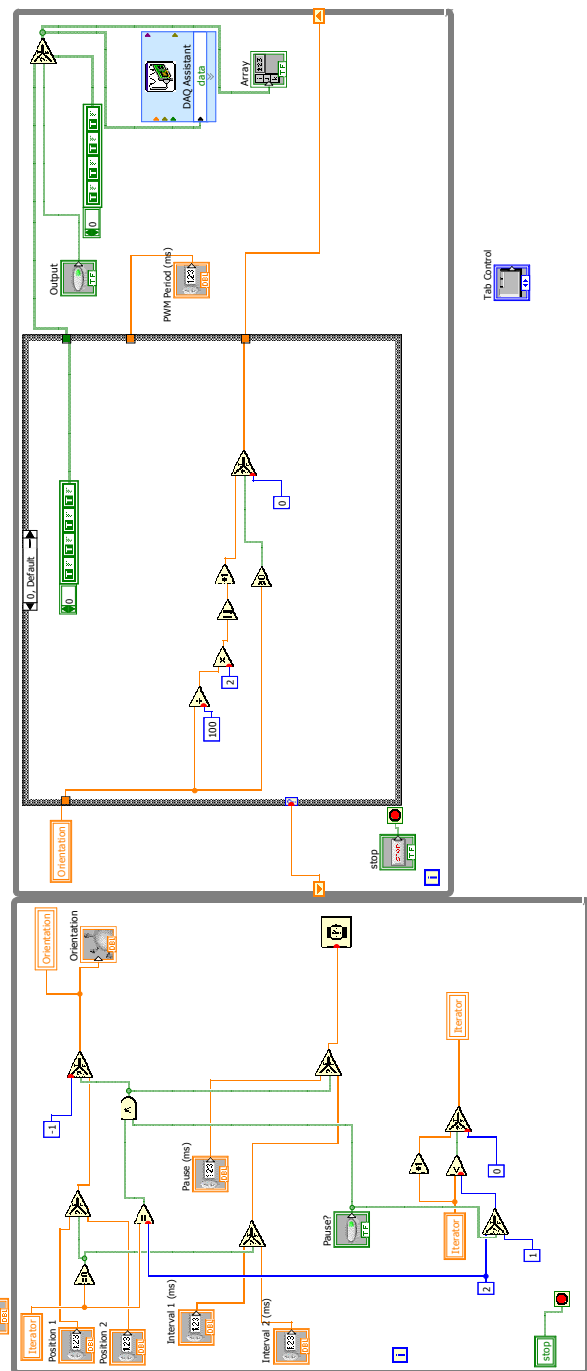Figure B1.2 - All 16 cases common to all operation modes.

Alternated.vi
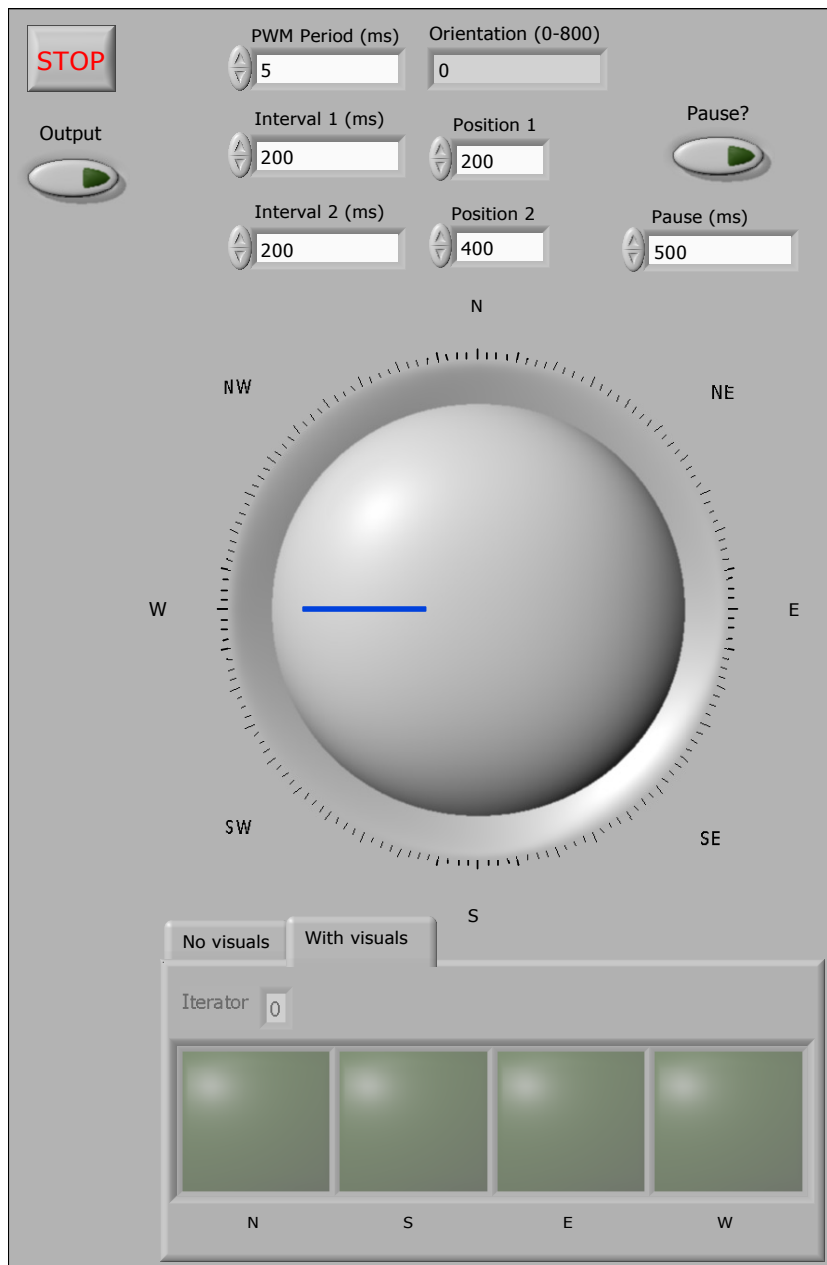
PWM Period (ms)
5

Orientation (0-800)
0

Interval 1 (ms)
200

Position 1
200

Pause?

Interval 2 (ms)
200

Position 2
400

Pause (ms)
500

N

NW

NE

W

E

SW

SE

S

No visuals | With visuals

Iterator 0

N   S   E   W

Figure B1.3 - Alternated Mode: control panel and source code.
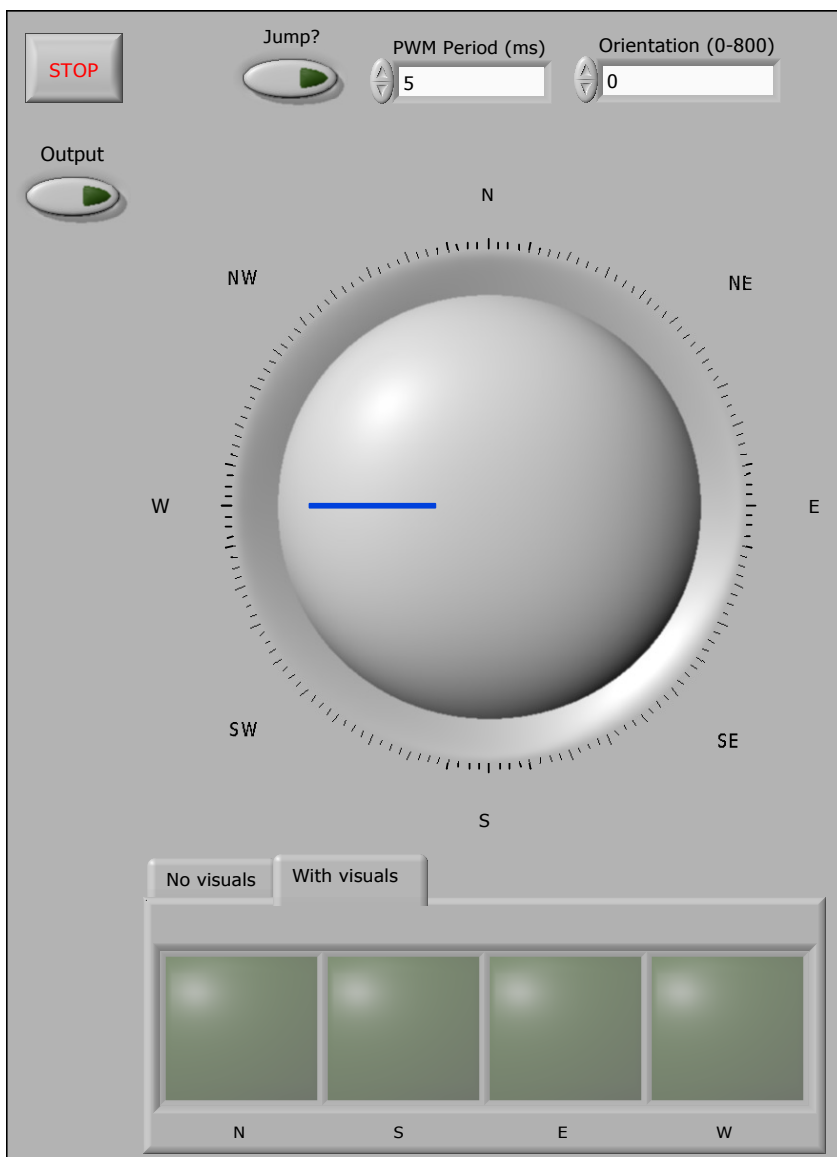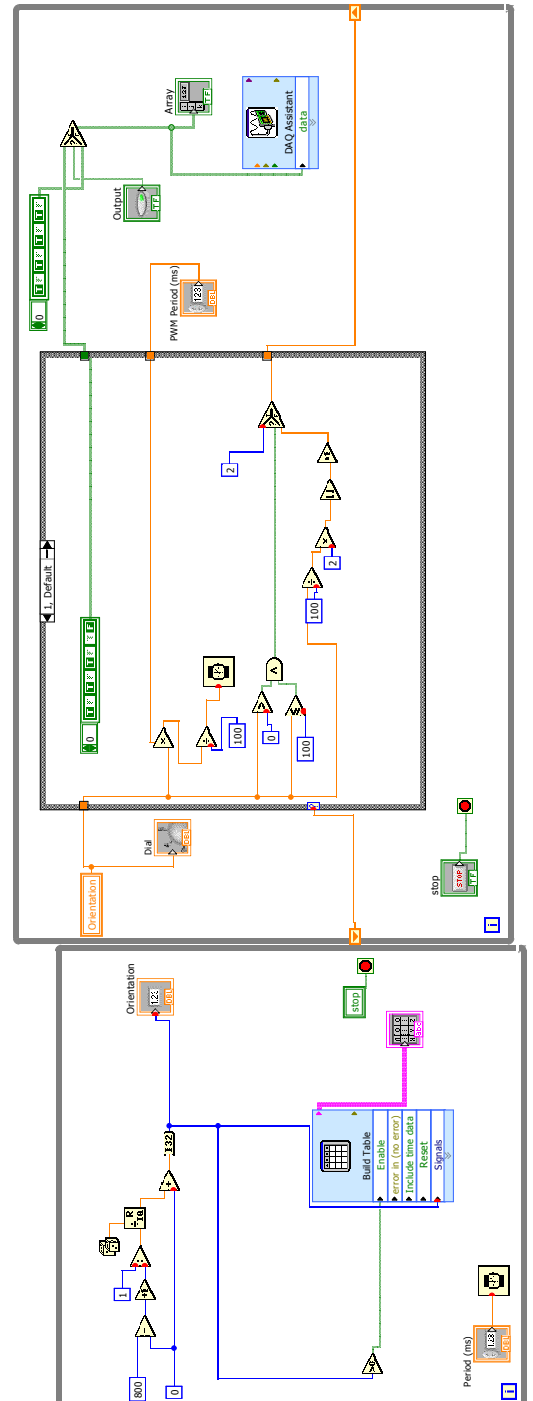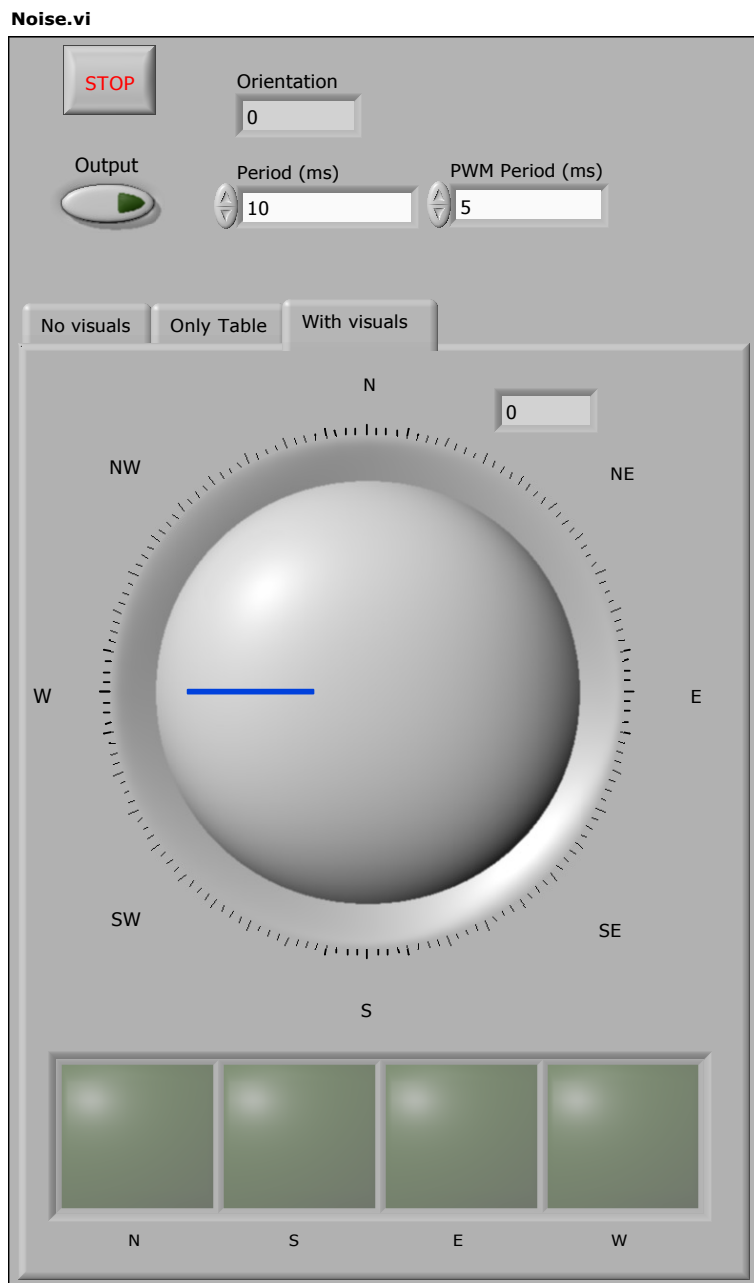
Manual.vi
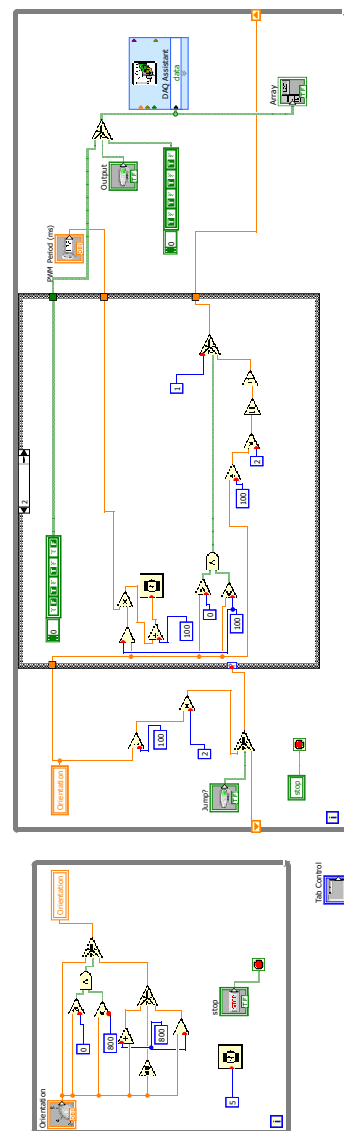
Figure B1.4 - Manual Mode: control panel and source code.

Figure B1.5 - Noise Mode: control panel and source code.